Precambrian Research 276 (2016) 145–157

Contents lists available at ScienceDirect

Precambrian Research

journal homepage: www.elsevier.com/locate/precamres

Extremely low oxygen concentration in mid-Proterozoic shallow seawaters

Dongjie Tang[a,b], Xiaoying Shi[a,c,*], Xinqiang Wang[a,c], Ganqing Jiang[d]

[a] State Key Laboratory of Biogeology and Environmental Geology, China University of Geosciences, Beijing 100083, China
[b] Institute of Earth Sciences, China University of Geosciences, Beijing 100083, China
[c] School of Earth Sciences and Resources, China University of Geosciences, Beijing 100083, China
[d] Department of Geoscience, University of Nevada, Las Vegas, NV 89154-4010, USA

ARTICLE INFO

Article history:
Received 4 September 2015
Received in revised form 4 January 2016
Accepted 12 February 2016
Available online 22 February 2016

Keywords:
Rare Earth Element (REE)
Cerium (Ce) anomaly
Shallow-marine oxygen concentration
Mid-Proterozoic ocean
Primitive eukaryotes
North China platform

ABSTRACT

The mid-Proterozoic (1.8–0.8 Ga) witnessed the first appearance but unusually low diversification of eukaryotes. The stagnant biotic evolution during this billion-year-long period (commonly referred to as the "Boring Billion") was arguably ascribed to low oxygen levels in atmosphere and ocean. However, evidence supporting low oxygen in shallow-marine environments where early eukaryotes first evolved is generally lacking or insufficient. Here we report Rare Earth Element and yttrium (REE + Y) data, particularly cerium (Ce) anomalies, from a suite of mid-Proterozoic sedimentary rocks of the North China platform. The new data from North China, in combination with available Ce anomaly data from other Proterozoic successions, demonstrate that during mid-Proterozoic, negative Ce anomalies did not occur until ~1.54 Ga and after ~1.54 Ga, only episodic negative Ce anomalies were present in shallow-water carbonates. Trace element enrichments (U_{EF}, V_{EF}, and Mo_{EF}) remained at the average continental crust level before ~1.54 Ga but showed a sudden increase at ~1.54 Ga. The data suggest that oxygen concentration in shallow-marine environments of the mid-Proterozoic ocean was extremely low, probably <0.2 μM prior to ~1.54 Ga (based on minimal oxygen concentration requirement for Ce(III) oxidation) and fluctuating around 0.2 μM afterwards. The low oxygen concentration (~0.2 μM) in shallow waters of the mid-Proterozoic ocean accounts for only ~0.1% of the modern surface ocean oxygen level (~280 μM) and may help explain the evolutionary stasis of eukaryotes during the mid-Proterozoic.

1. Introduction

Increasing evidence in the last decade has shown that the oxygenation of Earth's surface environments occurred at the beginning and end of the Proterozoic (Och and Shields-Zhou, 2012; Lyons et al., 2014). During the Great Oxidation Event (GOE; Holland, 2002) around 2.4 Ga (e.g., Bekker et al., 2004), atmospheric oxygen may have increased from <0.001% present atmospheric level (PAL) in Archean to >0.1% PAL (e.g., Farquhar et al., 2000; Pavlov and Kasting, 2002; Holland, 2006) in Paleoproterozoic, resulting in stratified oceans with possibly oxic surface water but ferruginous or euxinic deep-water (e.g., Canfield, 1998; Planavsky et al., 2011; Reinhard et al., 2013; Lyons et al., 2014). During the Neoproterozoic Oxygenation Event (NOE; Och and Shields-Zhou, 2012) between 800 and 542 Ma (e.g., Fike et al., 2006; Canfield et al., 2007; Scott et al., 2008; Sahoo et al., 2012; Kendall et al., 2015), atmospheric oxygen level further increased (e.g., Canfield and Teske, 1996; Holland, 2006; Lyons et al., 2014), leading to well-oxygenated shallow-waters and variably oxygenated deep-waters in the ocean (e.g., Canfield et al., 2008; Johnston et al., 2013; Kurzweil et al., 2015; Sperling et al., 2015).

The mid-Proterozoic (1.8–0.8 Ga) between GOE and NOE is an intriguing period in Earth history that witnessed the first appearance but unusually low diversity of primitive eukaryotes (Han and Runnegar, 1992; Rasmussen et al., 2008). Although some multicellular eukaryotes appeared during the late Mesoproterozoic (Woods et al., 1998; Butterfield, 2000, 2001), the evolution of eukaryotic organisms was apparently stagnant (Knoll et al., 1995, 2006; Javaux et al., 2001; Lamb et al., 2009) and their abundance was very low (Brocks et al., 2005; Blumenberg et al., 2012; Reinhard et al., 2013). This billion-year-long period of evolutionary stasis, commonly referred to as the "Boring Billion", was thought to be related to low oxygen levels in atmosphere and ocean (e.g., Anbar and Knoll, 2002; Canfield, 2005; Knoll et al., 2006; Kump, 2008;

* Corresponding author at: State Key Laboratory of Biogeology and Environmental Geology, China University of Geosciences, Beijing 100083, China. Tel.: +86 10 82321737; fax: +86 10 82321737.
E-mail addresses: dongjtang@126.com (D. Tang), shixyb@cugb.edu.cn (X. Shi).

http://dx.doi.org/10.1016/j.precamres.2016.02.005
0301-9268/

Reinhard et al., 2013; Smith and Harper, 2013; Luo et al., 2014; Planavsky et al., 2014; Gilleaudeau and Kah, 2015), although some have argued that the evolution of life is intrinsically controlled and independent of surface oxygenation (e.g., Butterfield, 2009; Erwin et al., 2011; Sperling et al., 2013; Mills et al., 2014).

The redox landscape of the mid-Proterozoic ocean, however, remains debated. Earlier studies suggested that the ocean was oxygenated after ~1.8 Ga, coincident with the disappearance of banded iron formation (BIF) (e.g., Holland, 2006). In another model, the mid-Proterozoic ocean was envisioned to be stratified and dominated by H_2S (euxinic conditions) in the deep ocean (Canfield, 1998). More recent studies demonstrated widespread iron-rich (ferruginous) conditions in the mid-Proterozoic ocean (Planavsky et al., 2011; Reinhard et al., 2013; Lyons et al., 2014). Estimation of mid-Proterozoic atmospheric O_2 level also varies significantly. Traditional pO_2 estimates of 1–40% PAL (e.g., Holland, 2002, 2006) were well above the oxygen demands of eukaryotes. More recent studies suggested that pO_2 may have declined significantly (to <0.1% PAL) after the GOE and remained at this level for more than a billion years (Bekker and Holland, 2012; Lyons et al., 2014; Planavsky et al., 2014). This extremely low (<0.1% PAL) pO_2 estimate raises questions about whether there was sufficient O_2 to oxidize surface ocean seawater and promote the diversification of eukaryotes. Answering these questions requires understanding the redox conditions of shallow-marine environments in the mid-Proterozoic ocean.

Rare Earth Elements and yttrium (REE + Y) data, particularly cerium (Ce) anomalies (expressed as $Ce/Ce^* = [Ce_{(SN)}/(Pr^2_{(SN)}/Nd_{(SN)})]$; Lawrence et al., 2006), provide a means of documenting shallow-marine redox conditions (e.g., Planavsky et al., 2010; Ling et al., 2013). Unlike other REEs that typically exist in a trivalent oxidation state, Ce is unique in that it can also exist in tetravalent oxidation state, depending on environmental redox conditions (de Baar et al., 1988; German and Elderfield, 1989; Sholkovitz and Schneider, 1991). In modern oxygenated seawater, Ce(III) is rapidly oxidized to Ce(IV) through mediation of manganese oxide and/or bacteria (Byrne and Sholkovitz, 1996; Tachikawa et al., 1999; Tanaka et al., 2010). Ce(IV) is absorbed by Fe–Mn nodules and crusts in oxygenated deep ocean (Elderfield et al., 1981; Bau et al., 1996), resulting in negative Ce anomalies in seawater and positive Ce anomalies in Fe–Mn oxides (Bau et al., 1996). Although Ce concentrations in shallow seawaters are highly variable (Kamber and Webb, 2001), highest Ce/Ce* values of the surface waters in modern oceans or seas are all less than 0.55 (Shimizu et al., 1994; Bertram and Elderfield, 1993; German et al., 1995; Nozaki et al., 1999; Slack et al., 2007). In anoxic oceans such as those in Archean and Paleoproterozoic, the lack of Ce(III) oxidation and absence of deep-ocean Fe–Mn oxides lead to high seawater Ce concentration. Therefore, no negative Ce anomaly is expected and Ce/Ce* values may be close to or higher than 1.0 (Kamber and Webb, 2001; Van Kranendonk et al., 2003). Although some negative Ce anomalies were reported from Archean sedimentary rocks, their veracity and depositional origin have been questioned (e.g., Planavsky et al., 2010). Intermediately oxygenated ocean may have Ce/Ce* values between 0.55 and 1 (e.g., Ling et al., 2013). Thus, secular Ce/Ce* record tracks first-order ocean redox changes in Earth history.

Within the envelope of secular Ce/Ce* record, Ce anomalies can also record local redox conditions. In redox-stratified environments (basins), reductive dissolution of settling Fe–Mn oxides below Fe–Mn redox boundaries lead to Ce(III) enrichments and higher Ce/Ce* values in deep waters below the chemocline (German et al., 1991; Byrne and Sholkovitz, 1996; Slack et al., 2007). In this case, lower Ce/Ce* values in shallow water environments at or above the chemocline are expected. When the entire water column has low level of dissolved oxygen (without highly oxygenated shallow waters), Ce redox-cycle may stop and differential Ce/Ce* values are not expected between shallow- and deep-water environments.

In this paper, we use Ce anomaly and REE patterns, along with redox-sensitive trace element enrichments (U, V, and Mo), to evaluate the redox evolution of shallow waters on the North China platform during the period of ca. 1.65–1.47 Ga. We also construct the secular Ce/Ce* record with available data from other Proterozoic successions. To date, the shallow-water redox state of the mid-Proterozoic ocean has not been sufficiently investigated, except for the recent study of Cr isotopes (Planavsky et al., 2014) and iodine concentrations of Achaean and early Paleoproterozoic carbonates (Hardisty et al., 2014). We aim at testing the hypothesis that the low oxygen level in surface ocean during mid-Proterozoic has prevented the diversification of early eukaryotes.

2. Geological setting

2.1. Regional geology

Associated with the break-up of supercontinent Columbia or Nuna (Zhao et al., 2003, 2004, 2011; Zhang et al., 2012) to the assembly of Rodinia (Li et al., 2008), a thick (~9000 m) sedimentary succession was deposited on the North China platform during the Proterozoic. This succession is commonly subdivided into three groups (Fig. 1) including the Changcheng Group (1800–1600 Ma, Pt_1), Jixian Group (1600–1400 Ma, Pt_2), and the Qingbaikou Group (1000–800 Ma, Pt_3), with a significant hiatus of ~400 Ma between the Jixian and Qingbaikou groups (Gao et al., 2009; Su et al., 2010; Li et al., 2013; Su, 2014).

The Changcheng Group is dominated by siliciclastic rocks that were deposited on the Archean-early Paleoproterozoic crystalline basement. This group, in stratigraphic order, includes the Changzhougou, Chuanlinggou, Tuanshanzi and Dahongyu formations. Alluvial to fluvial conglomerates and sandstones constitute the basal part of the group, representing deposition associated with the initial regional extension (Lu et al., 2002, 2008). Ironstones and black shales of the Chuanlinggou Formation probably record the initial breakup of the Columbia supercontinent and a rapid basement subsidence (Zhao et al., 2011; Tang et al., 2015). The Jixian Group includes the Gaoyuzhuang, Yangzhuang, Wumishan, Hongshuizhuang and Tieling formations and is dominated by carbonate rocks including laminated and stromatolitic dolostone, limestone, argillaceous dolostone and chert bands. The thick carbonate succession was likely deposited from an epicontinental sea. Above the Jixian Group, a regional unconformity is observed across the entire North China platform (Qiao et al., 2007; Su et al., 2010). The overlying Xiamaling Formation consists mainly of organic-rich black shales that were likely deposited from low-energy environments of an intra-shelf basin (Qiao et al., 2007; Luo et al., 2014). Unconformably overlying the Xiamaling Formation is siliciclastic and carbonate rocks of the Changlongshan and Jing'eryu formations of the Qingbaikou Group. A significant uplift after the Jing'eryu Formation exposed the Proterozoic strata until the middle Cambrian (Zhou et al., 2006), which is commonly thought to have resulted from the formation of supercontinent Rodinia (Wang et al., 2000; Lu et al., 2008).

The mid-Proterozoic strata are well preserved on the North China platform, with low metamorphism commonly below prehnite–pumpellyite phase (Li et al., 2003; Chu et al., 2007). The low metamorphism of rocks warrants that REE + Y signatures may record their primary signals (Bau and Möller, 1993) and can be used for paleoenvironmental interpretation (e.g., Planavsky et al., 2010; Ling et al., 2013).

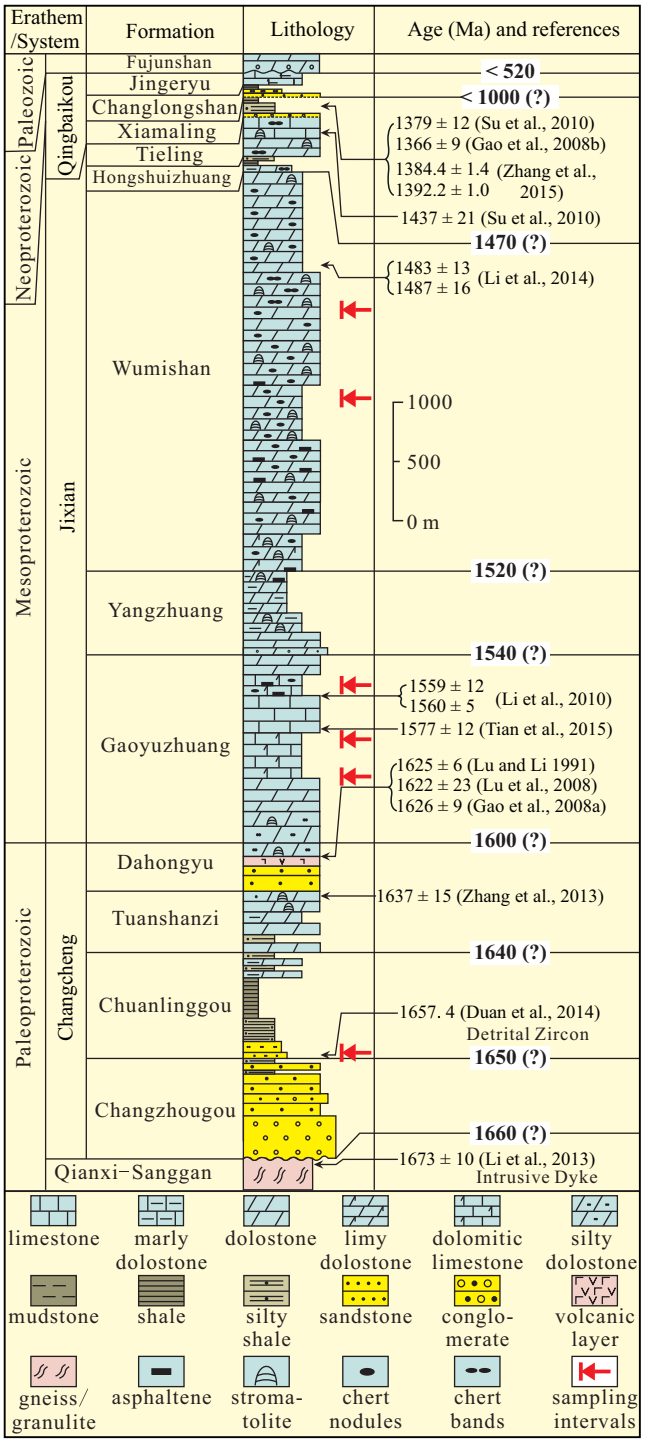

Fig. 1. Generalized stratigraphic subdivisions and zircon U–Pb age constraints of the Proterozoic succession on the North China platform. The thickness of stratigraphic units varies by location. Question marks indicate estimated boundary ages on the basis of existing U–Pb ages and stratigraphic thicknesses.

2.2. Geochronological framework

In recent years, a number of zircon U–Pb ICP–MS, SHRIMP and TIMS ages have been obtained from the Proterozoic succession of the North China platform (Lu and Li, 1991; Li et al., 2010, 2013, 2014; Gao et al., 2007, 2008a, 2008b; Lu et al., 2008; Su et al., 2008, 2010; Zhang et al., 2013, 2015; Duan et al., 2014; Su, 2014; Tian et al., 2015), which provide reasonable geochronologic constraints to the stratigraphic units (Fig. 1). Based on the radiometric ages and stratigraphic relationships, the base and top of the Chuanlinggou Formation can be defined at ~1.65 Ga and ~1.64 Ga; those for the Gaoyuzhuang Formation can be set at ~1.60 and ~1.54 Ga; and those for the Wumishan Formation are placed at ~1.52 Ga and ~1.47 Ga, respectively (Qiao et al., 2007; Gao et al., 2009, 2010; Li et al., 2010, 2013; Tang et al., 2015).

2.3. Sedimentary facies

Our ironstone samples were collected from the lower part of the Chuanlinggou Formation, and carbonate samples were from the Gaoyuzhuang and Wumishan formations in Hebei province and the suburb of Beijing (Fig. 2). Regionally, the Chuanlinggou Formation is dominated by black shale and dark gray silty mudstone deposited from low-energy subtidal environments (Li et al., 2003, 2015; Chu et al., 2007). However, in the sampling sites (Xuanhua and Chicheng, Hebei province), Member-I of this formation is characterized by oolitic and stromatolitic ironstones (Fig. 3A and B) with some hematite-rich sandstone interbeds, and was mainly deposited from shallow subtidal environments (Dai et al., 2004; Tang et al., 2015).

The Gaoyuzhuang Formation is predominated by carbonates and can be divided into four members in the Yanqing area, suburb of Beijing. Member-I consists of sandstones with cross-bedding in the lower part and stromatolitic dolostones in the upper part. This Member was thought to have deposited from shallow subtidal to intertidal environments (Mei, 2008). Member-II consists of manganiferous dolostone in the lower part, with some Mn-concretion-bearing dark shale interbeds of subtidal origin (Mei, 2008), and thick-bedded muddy dolostone in the upper part, from which evidence of subaerial exposure indicates intertidal to supratidal environments (Fig. 3C). The lower part of Member-III is composed of thin-bedded muddy dolostone without any wave-influenced structures (Fig. 3D) and calcareous mudstone with cm- to dm-sized carbonate concretions (Fig. 3E). The lack of wave- and tide-influenced structures suggests deposition from low-energy deep-water environments possibly below storm wave base (Mei, 2007, 2008; Guo et al., 2010, 2013a; Luo et al., 2014, 2015). The middle part of Member III contains thick-bedded thrombolites (Fig. 3F) and the upper part consists of microbially-laminated dolostones (Fig. 3G). These features are interpreted as deposition from shallow subtidal to intertidal environments (Guo et al., 2010). Member-IV of the Gaoyuzhuang Formation is characterized by massive microbial reef carbonates with a total thickness up to 450 m (Mei, 2007, 2008). The presence of conical stromatolite (*Conophyton*) (Fig. 3H) and thinly laminated microbialites (Fig. 3I, cf. Bartley et al., 2015) in this member indicates deep-water environments, at least episodically below fair-weather wave base.

The Wumishan Formation is dominated by peritidal dolostones with abundant chert bands and various microbialites (Tang et al., 2013a). This formation is divided into four members. Member-I is composed of oolitic, stromatolitic and micritic dolostones that were mostly deposited in shallow subtidal to intertidal environments. Member-II consists mainly of tabular thrombolites with some intraclasts and thickly bedded dolostones of shallow subtidal to intertidal environments. Member-III contains thick-bedded domal and tabular thrombolites devoid of wave-influenced structures indicative of deep subtidal environments and layered stromatolitic dolostones of shallow subtidal origin. Member-IV is made up of micritic and finely-laminated dolostones, with thin layers of thrombolitic dolostone in its lower part. The thrombolites are gradually substituted by stromatolites in the upper part, showing a shallowing-upward trend formed in a prograding carbonate platform (Shi et al., 2008; Tang et al., 2011, 2013a). This formation is highly cyclic, with subtidal–intertidal–supratidal facies organized into meter-scale parasequences (cycles). A typical parasequence

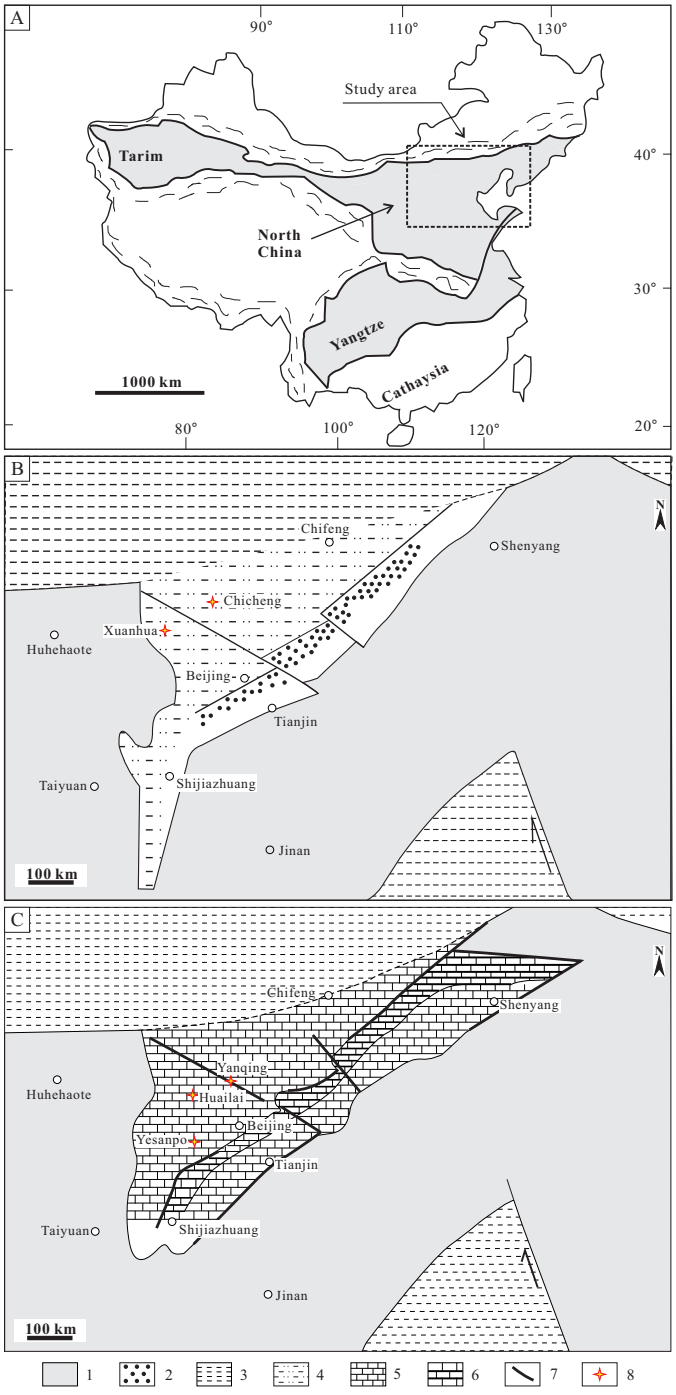

Fig. 2. (A) Major tectonic subdivisions of China, showing the study area (square). (B) Paleogeography of the North China platform during deposition of the Chuanlinggou Formation (late Paleoproterozoic). (C) Paleogeography of the North China platform during deposition of the Gaoyuzhuang and Wumishan formations (middle Mesoproterozoic). Modified from Qiao and Gao (2007) and Qiao et al. (2007). Legends: 1 – exposed area; 2 – coarse-grained siliciclastic-dominated rocks; 3 – deep-water siliciclastic-dominated rocks; 4 – shallow-water mudstone; 5 – shallow-water carbonate; 6 – deep-water carbonate; 7 – fault; 8 – sampled sections.

has subtidal thrombolite in the low part (Fig. 3J), shallow subtidal to intertidal microbial mat-rich micritic dolostone (Fig. 3K) in the middle part, and supratidal argillaceous dolostone with exposure surfaces in the upper part (Fig. 3L, Tang et al., 2013a). Dark biolaminites sampled from Member-II were interpreted to have formed in a submarine lagoonal environment (Tang et al., 2014).

3. Materials and methods

Samples analyzed in this study were collected from several formations covering different lithologies. Oolitic and stromatolitic ironstones were collected from Member-I of the Chuanlinggou Formation at the Sanchakou section (N: 40°48′05.01″, E: 115°40′27.76″) in Chicheng County and the Majiayao section (N: 40°39′38.54″, E: 115°8′25.12″) in Xuanhua County of Hebei Province. Dolostone samples were collected from the upper parts of Member-II and Member-III of the Gaoyuzhuang Formation at the Gan'gou section (N: 40°39′49.5″, E: 116°14′30.2″) in Yanqing County, suburb of Beijing. Microbial reef carbonates of the Gaoyuzhuang Member-IV were collected from the Gan'gou (N: 40°39′18.984″, E: 116°14′26.711″) and Malugou sections (N: 40°44′28. 524″, E: 116°12′37.645″) in Yanqing County, suburb of Beijing. Dolostone samples of the Wumishan Formation were collected from Yesanpo (N: 39°39′45″, E: 115°27′40″) and Huailai (N: 40°28′00″, E: 115°27′01″) in Hebei Province and from the Western Hills (N: 40°02′50″, E: 115°49′33″) of Beijing.

Samples were cut into chips and thin sections, and they were petrographically examined and photographed. Well-preserved samples were selected for REE + Y analysis. In preparation for REE + Y analyses, polished chips were drilled for powders, avoiding weathered surfaces, fractures, and recrystallized areas.

Previous studies indicated that non-skeletal carbonates and ironstones can record seawater REE + Y patterns (e.g., Webb and Kamber, 2000; Kamber and Webb, 2001; Nothdurft et al., 2004; Planavsky et al., 2010), but they are vulnerable to contamination from terrigenous sediments, particularly clay minerals (e.g., Van Kranendonk et al., 2003; Olivier and Boyet, 2006; Planavsky et al., 2010; Ling et al., 2013). Existing REE + Y data in literature were produced using a variety of acids, including nitric acid (Webb and Kamber, 2000), hydrochloric acid (Banner et al., 1988), sodium acetate mediated with acetic acid (Tessier et al., 1979), and acetic acid (Nothdurft et al., 2004; Ling et al., 2013). Usually, for pure carbonate nitric acid and/or hydrochloric acid were used, whereas for impure carbonate rocks sodium acetate–acetic acid or simply acetic acid was used. We used hydrochloric acid to digest ironstone samples because acetic acid cannot efficiently dissolve hematite and HF/HNO_3 to digest pure carbonate samples because detrital contamination is negligible. We used acetic acid to dissolve impure carbonates for avoiding contamination from terrigenous components.

For carbonate samples with terrigenous components, about 0.05 g sample powders were placed in a 50 mL centrifuge tube, followed by addition of ~40 mL DI water and 500 ng Rh internal standard. Next, 2.5 mL acetic acid (98%, purified by sub-boiling) was added to dissolve the carbonate. When the solution is no longer bubbling, it was diluted to 50 mL and sealed. The sealed tube was shaked for about 1 h and then centrifuged for 3 min at 3000 rpm. The solution without insoluble residue was used to measure REEs and trace elements. The preparation process for ironstone samples is similar, but the acid used to dissolve sample powders was 4 M HCl. REEs and trace elements were analyzed using a Bruker Aurora M90 ICP-MS at the Institute of Geochemistry, Chinese Academy of Sciences. For pure carbonate samples, a mixture of 6 N HF and 6 N HNO_3 (1:2) was used to dissolve sample powders following the methods described in Guo et al. (2013b). The solution was used to measure REEs and trace elements using a Finnigan MAT HR-ICP-MS (Element 1) at Beijing Geological Research Institute of China National Nuclear Corporation. We used ^{151}Eu and ^{157}Gd to monitor the measurement. The interferences of $^{135}Ba^{16}O$ to ^{151}Eu and $^{141}Pr^{16}O$ to ^{157}Gd were corrected by measuring the standard solution of 400 ppb Ba and 40 ppb Pr. The average Ba concentration of all our samples is 10.463 ppm (0.561–69.900 ppm), which are significantly lower than that of the reference materials

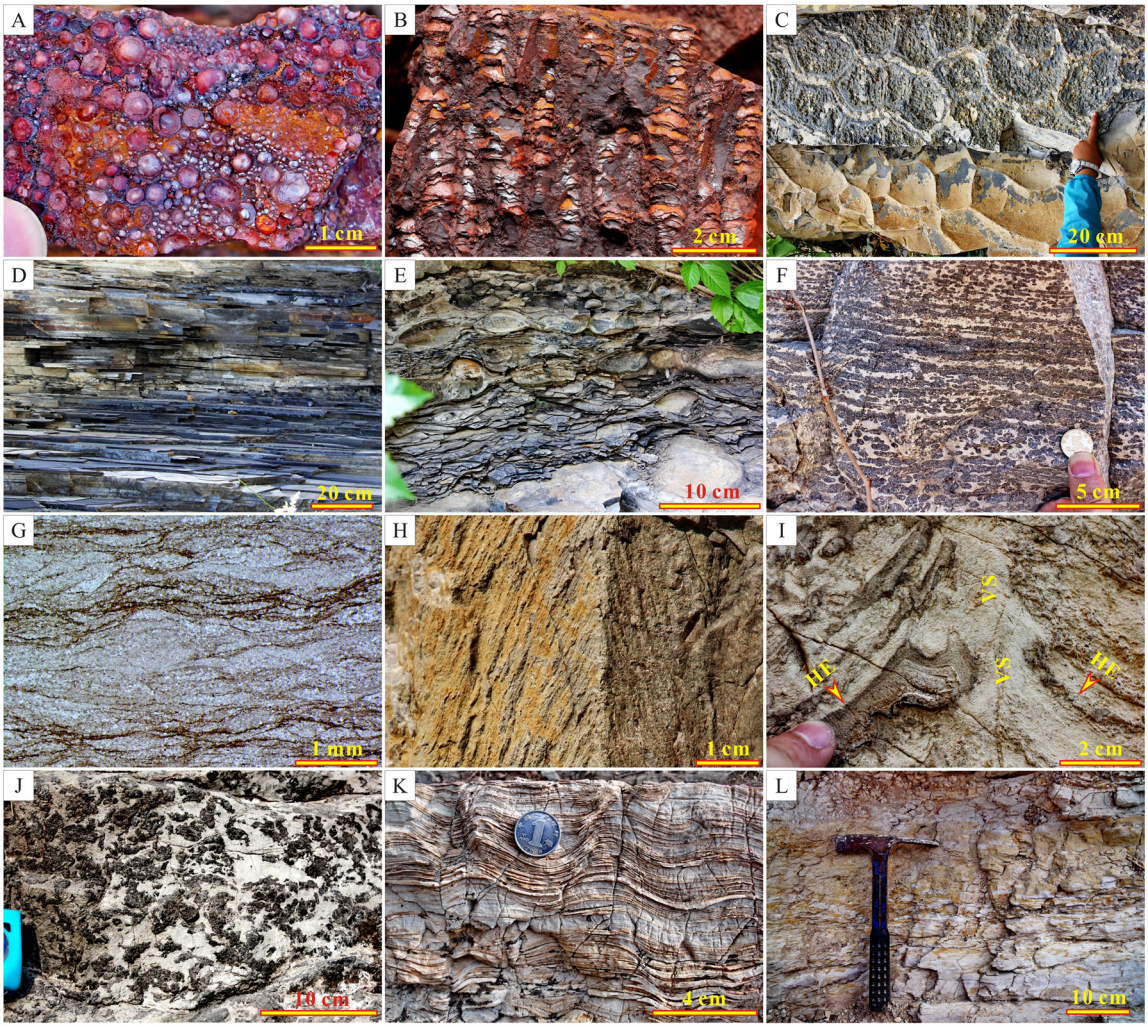

Fig. 3. Some common lithologies and sedimentary structures indicative of depositional environments in studied sections. (A) Oolitic ironstone from Member-I of the Chuanlinggou Formation, Chicheng. (B) Stromatolitic ironstone from Member-I of the Chuanlinggou Formation, Chicheng. (C) Medium-bedded muddy dolostone with mudcracks on bedding surface, Member-II of the Gaoyuzhuang Formation, Yanqing. (D) Thinly-bedded dark-gray muddy dolostone without current-influenced structures, Member-III of the Gaoyuzhuang Formation, Yanqing. (E) Cm- to dm-sized carbonate concretions in calcareous mudstone, Member-III of the Gaoyuzhuang Formation, Yanqing. (F) Massive thrombolites with mm-scale mesoclots, Member-III of the Gaoyuzhuang Formation, Yanqing. (G) Photomicrograph showing microbially-laminated dolostones with wavy laminations, Member-III of the Gaoyuzhuang Formation. (H) Conical stromatolite (*Conophyton*) from Member-IV of the Gaoyuzhuang Formation, Yanqing. (I) Microbialites with positive relief expressed by near vertical ridges (VS) and sub-horizontal drapes (HE), Member-IV of the Gaoyuzhuang Formation, Yanqing. (J) Massive thrombolites with mm- to cm-sized mesoclots, Member-III of the Wumishan Formation, Yesanpo. (K) Laminated microbial mats and micritic dolostone from Member-III of the Wumishan Formation, Yesanpo. (L) Argillaceous dolostone from Member-III of the Wumishan Formation, Huailai.

(322.3–908.00 ppm), indicating that the Ba interference on REE + Y of our samples is negligible. Reference materials AMH-1 (andesite), BCR-2 (basalt), GBPG-1 (plagiogneiss) and OU-6 (slate) are used to monitor the precision and reproducibility. The precision of all ICP-MS analyses is better than ±5–10% (relative) for most analyzed elements. More specifically, the precision for elements V, Mo, Cr, Th, U, Y, Ba, La, Ce, Eu, Gd, Tb, Tm, Yb and Lu is better than ±10% (relative) and for Pr, Nd, Sm, Dy, Ho and Er, it is better than ±5% (relative).

4. Results

In this study, 79 samples from early mid-Proterozoic strata of the North China platform were analyzed for REE + Y and redox-sensitive trace element (RSE) concentrations. The results are listed in Table S1 and illustrated in Figs. 4–8. We also compiled the secular Ce/Ce* variations through time (Fig. 8) using available data in literature (Table S1; Kato et al., 1996, 1998, 2002; Alibo and Nozaki, 1999; Webb and Kamber, 2000; Nothdurft et al., 2004; Alexander et al., 2008; Azmy et al., 2009; Planavsky et al., 2010; Ling et al., 2013; Tang et al., 2013b).

In general, all analyzed samples show little contamination from clastic components and have seawater-like REE + Y patterns when normalized to Post-Archean Australian Shale (PAAS) (Fig. 4). Ironstone samples from the Chuanlinggou Formation have REE and Th concentrations of 6.133–124.963 ppm and 0.633–2.212 ppm, respectively, which are similar to those in Banded Iron Formations (BIFs) with low clastic contents (e.g., Planavsky et al., 2010). Carbonate samples have much lower REE and Th concentrations of 0.58–47.841 ppm and 0.002–1.415 ppm, respectively. They are similar to those in microbialites without clastic contamination (e.g., Nothdurft et al., 2004). No co-variation between Ce/Ce*, $Pr_{(SN)}/Yb_{(SN)}$, Y/Ho ratios and Th concentrations is observed (Fig. 5).

Ling et al. (2013) suggested using Th concentrations (Th <0.5 ppm) as a criterion to screen samples with siliciclastic contamination. Using this criterion, samples from the Chuanlinggou Formation and Member-II of the Gaoyuzhuang Formation, and part of the samples from Member-III of the Gaoyuzhuang Formation

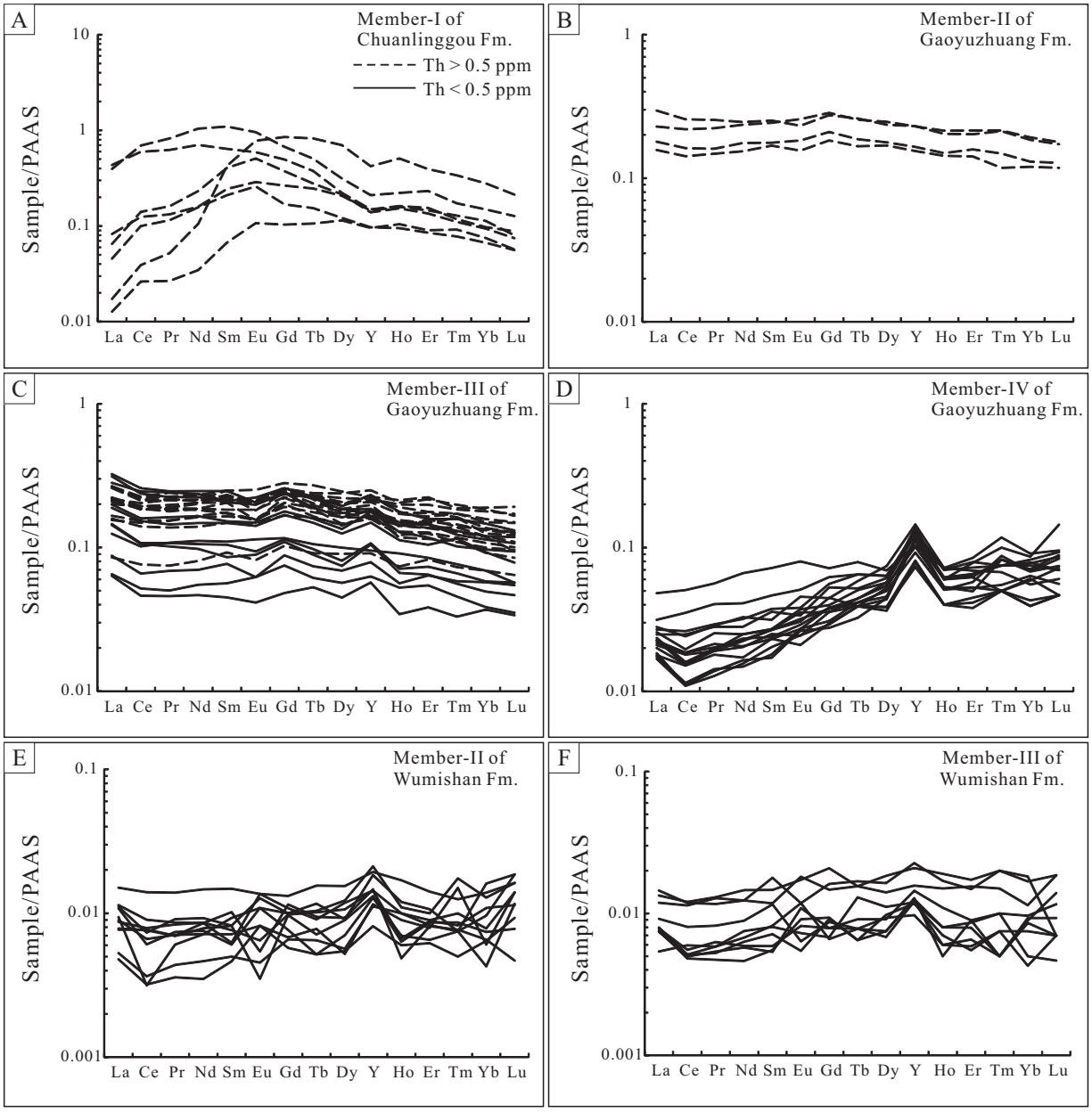

Fig. 4. PAAS-normalized REE patterns for ca. 1.65–1.47 Ga ironstone and carbonate samples from the North China platform.

are deemed to be contaminated by siliciclastic components. However, the general trends of Th-screened Ce anomalies, $Pr_{(SN)}/Yb_{(SN)}$ and Y/Ho ratios, and enrichment factors of U, V, and Mo (calculated by $X_{EF} = (X/Th)_{sample}/(X/Th)_{upper\ crust}$; X represents U, V, and Mo) are virtually the same as those of unscreened dataset (Figs. 6 and 7), suggesting that siliciclastic influence on the REE + Y and RSE values are insignificant. Similar to modern seawater, PAAS-normalized REE + Y patterns of our samples show positive La anomalies (1.38 ± 0.45), none to moderately positive Gd anomalies (1.08 ± 0.19), and none to moderately positive Eu anomalies (1.10 ± 0.42).

Several temporal trends of REE + Y patterns and RSE enrichment factors are observed (Figs. 6 and 7). First, there are no statistically significant negative Ce anomalies observed until Member-IV of the Gaoyuzhuang Formation (~1.54 Ga, Fig. 6A). In this study, Ce anomalies were calculated using the equation $Ce/Ce^* = Ce_{(SN)}/[Pr_{(SN)}{}^2/Nd_{(SN)}]$ as suggested by Lawrence et al. (2006). Because of positive La in seawater, the conventional calculation ($Ce/Ce^* = 2^*Ce_{(SN)}/[La_{(SN)} + Pr_{(SN)}]$) would result in apparent negative or false Ce anomalies (Bau and Dulski, 1996; Lawrence et al., 2006). As shown in Fig. 6A, samples from Member-I of the Chuanlinggou Formation have Ce/Ce* values of 1.53–1.06 (1.22 ± 0.16) and those from Member-II and Member III of the Gaoyuzhuang Formation has Ce/Ce* values of 1.11–0.97 (1.03 ± 0.06) and 1.13–0.91 (1.02 ± 0.06), respectively. In contrast, samples from Member-IV of the Gaoyuzhuang Formation have lower Ce/Ce* values between 1.06 and 0.76 (0.94 ± 0.09). Member-II of the Wumishan Formation have Ce/Ce* values varying between 1.35 and 0.61 (0.95 ± 0.20) and Member-III of the same formation have Ce/Ce* values of 1.32–0.66 (1.01 ± 0.16). In other words, recognizable negative Ce anomalies appeared suddenly in Member-IV of the Gaoyuzhuang Formation, and episodic negative Ce anomalies are present in the overlying Wumishan Formation. The negative Ce/Ce* shift reported here is similar to that occurred in 2.33–2.06 Ga and in the latest Neoproterozoic (Fig. 8), both of which were interpreted as the result of increased ocean oxygenation (Tang

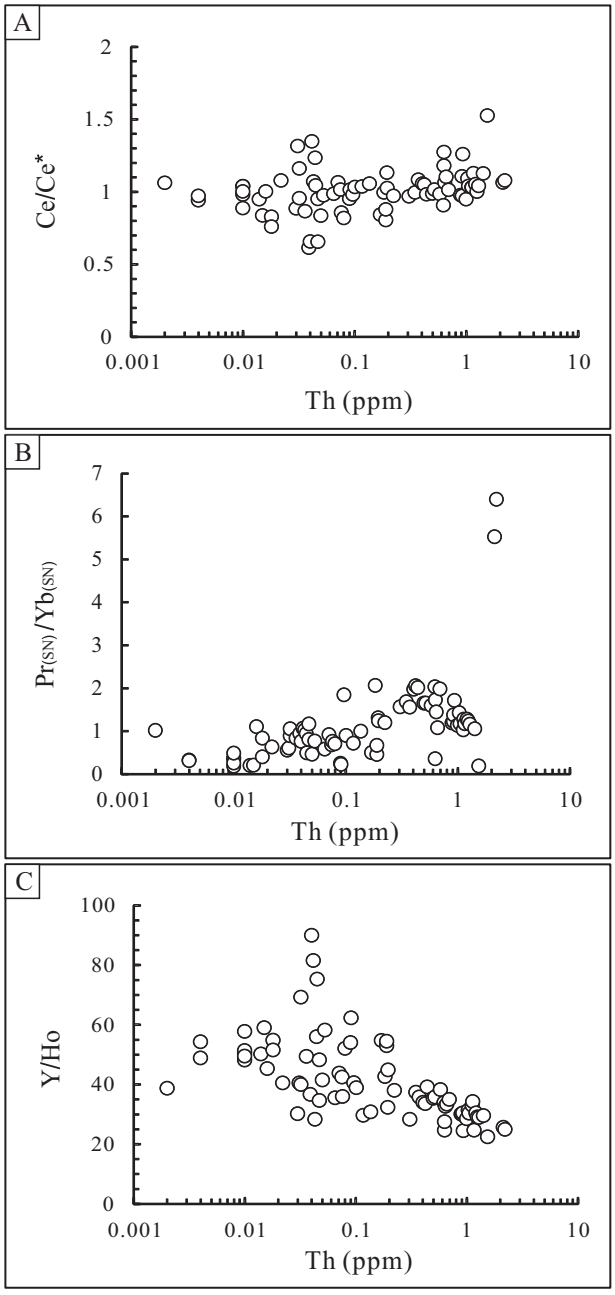

Fig. 5. Cross-plots of REE versus Th concentration of the ironstones and carbonates from the North China Platform. (A) Ce anomalies versus Th. (B) $Pr_{(SN)}/Yb_{(SN)}$ ratios versus Th. (C) Y/Ho ratios versus Th.

et al., 2013b; Ling et al., 2013). However, negative shifts in Ce/Ce* seem not to be unidirectional; more than half of the samples from Member-IV of the Gaoyuzhuang Formation and its overlying Wumishan Formation have Ce/Ce* values close to or slightly higher than 1, which are distinct from those of the latest Neoproterozoic and Phanerozoic strata (Fig. 8).

Second, carbonates (≤1.54 Ga) from Member-IV of the Gaoyuzhuang Formation and its overlying Wumishan Formation have much lower light-to-heavy REE ratios than carbonates from the lower Gaoyuzhuang Formation. Light-to-heavy REE ratios are represented by $Pr_{(SN)}/Yb_{(SN)}$ ratios. Samples from Member-IV of the Gaoyuzhuang Formation, and Member-II and III of the Wumishan Formation have average $Pr_{(SN)}/Yb_{(SN)}$ ratios of 0.39 ± 0.21, 0.85 ± 0.20, and 0.79 ± 0.19, respectively; while Member-II and III of the Gaoyuzhuang Formation have higher average $Pr_{(SN)}/Yb_{(SN)}$ ratios of 1.25 ± 0.09 and 1.52 ± 0.35, respectively (Fig. 6C). The ironstones from the Chuanlinggou Formation have highly variable $Pr_{(SN)}/Yb_{(SN)}$ ratios of 2.44 ± 2.49 (Fig. 6C).

Third, there is a significant increase in Y/Ho ratios in Member-IV of the Gaoyuzhuang Formation (~1.54 Ga) and its overlying Wumishan Formation (Fig. 6E). Carbonate samples from these units have an average Y/Ho ratio of 49.24 ± 13.32, which is markedly higher than the PAAS composite ratio of ~27. In contrast, carbonates and ironstones older than Gaoyuzhuang Member IV have lower average Y/Ho ratios of 32.19 ± 5.28.

The U, V, and Mo enrichment factors (U_{EF}, V_{EF}, and Mo_{EF}) of samples older than ~1.54 Ga are close to those of the average upper continental crust, while samples younger than ~1.54 Ga have higher U_{EF}, V_{EF}, and Mo_{EF} values (Fig. 7). To minimize the influence of siliciclastic components, RSE concentrations were normalized by Th concentration (cf. Schröder and Grotzinger, 2007). Member-I of the Chuanlinggou Formation and Member-II and III of the Gaoyuzhuang Formation have normalized U_{EF} values of 2.05 ± 0.67, 0.70 ± 0.20, and 1.73 ± 0.88, respectively; while Member-IV of the Gaoyuzhuang Formation, and Member-II and III of the Wumishan Formation have higher U_{EF} values of 32.93 ± 46.90, 9.17 ± 5.72, and 22.11 ± 19.33, respectively. The V_{EF} values also show an increase in Member IV of the Gaoyuzhuang Formation and its overlying Wumishan Formation (0.55 ± 0.28, 0.36 ± 0.09, and 0.83 ± 0.49 in Chuanlinggou Member-I, Gaoyuzhuang member-II and III, respectively, and 97.12 ± 154.24, 13.10 ± 8.54, and 25.25 ± 18.64 in Gaoyuzhuang Member-IV, Wumishan Member-II and III, respectively). Similarly, Mo_{EF} values increase in Gaoyuzhuang Member-IV and its overlying strata (0.17 ± 0.05, 0.33 ± 0.08, and 3.78 ± 5.37 in Chuanlinggou Member-I, Gaoyuzhuang Member-II and III; and 157.88 ± 251.26, 5.66 ± 3.67, and 17.80 ± 11.50 in Gaoyuzhuang Member-IV, and Wumishan Member-II and III, respectively).

5. Discussions

5.1. Evaluation of REE + Y anomalies

Because REE + Y contents in sediments (and sedimentary rocks) are much higher than those in diagenetic, metamorphic, and hydrothermal fluids, it has been suggested that REE + Y in Fe oxide-rich sediments and non-skeletal carbonates are rock buffered under low water/rock ratios in typical diagenetic and metamorphic conditions (e.g., Bau, 1993; Bau and Dulski, 1996; Kato et al., 1998; Slack et al., 2007). For example, even under intense weathering that destroyed the original rock textures, some REE anomalies (e.g., Eu anomaly) are still preserved (Nesbitt, 1979). Given that the Mesoproterozoic strata of the North China platform are well preserved and have a metamorphic grade below prehnite–pumpellyite phase (Li et al., 2003; Chu et al., 2007), we argue that diagenetic and metamorphic alteration on the REE + Y values of our samples may be minor.

Siliciclastic components (particularly clay minerals) may cause changes in REE + Y patterns in carbonate and Fe oxide-rich sediments (Kamber and Webb, 2001; Nothdurft et al., 2004; Planavsky et al., 2010). In our samples, the Th contents are very low in general (Fig. 5) and the Th-calibrated REE patterns are similar to those un-calibrated REE patterns. For example, the Th contents of HF/HNO_3-dissolved carbonate samples are in the range of 0.002–0.190 ppm (0.054 ppm in average), which only account for 0.37% (0.00–1.30%) of the Th value of PAAS. Further, there is no co-variation between Ce/Ce*, $Pr_{(SN)}/Yb_{(SN)}$, and Y/Ho ratios. Thus, we believe that siliciclastic contributions to the REE + Y patterns of our samples are insignificant.

Basin isolation may cause systematic changes in REE + Y anomalies. Sedimentological studies indicated that during deposition of the Gaoyuzhuang Formation and its underlying strata, the North

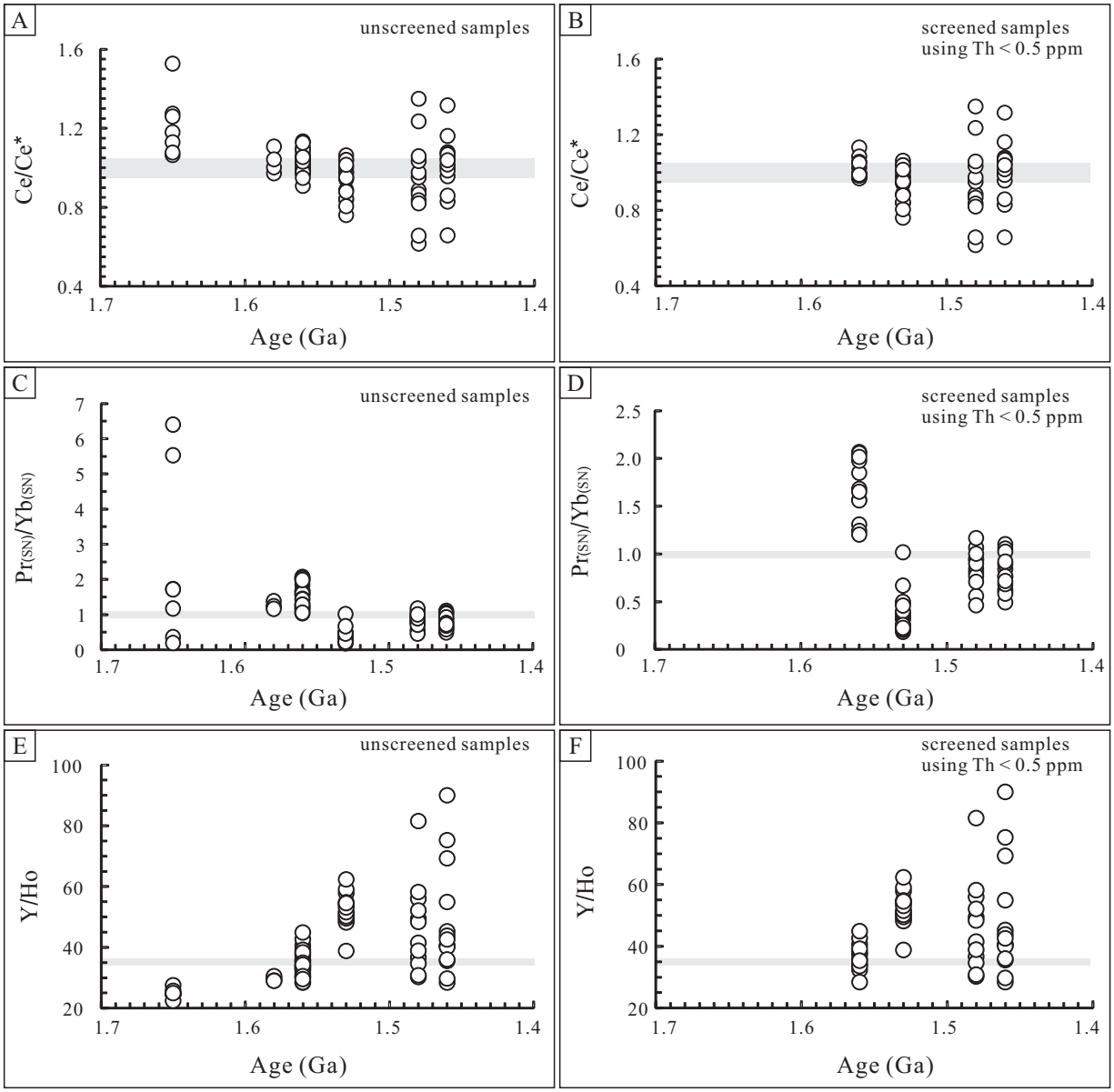

Fig. 6. Temporal trends of REEs of ca. 1.65–1.47 Ga ironstone and carbonate samples. (A) and (B) Ce anomalies, showing a negative shift of Ce anomalies at ~1.54 Ga. (C) and (D) Light to heavy REE ratios (represented by $Pr_{(SN)}/Yb_{(SN)}$), showing a decrease at ~1.54 Ga. (E) and (F) Y/Ho ratios showing an increase at ~1.54 Ga. Notice that Th-screened samples (using Th >0.5 ppm; Ling et al., 2013) show identical patterns with unscreened samples. Gray bar indicates PAAS shale composite values.

China platform was most likely connected to the open ocean (Mei, 2007, 2008; Guo et al., 2010, 2013a; Tang et al., 2013a, 2015). During deposition of the Wumishan Formation, local restriction in lagoonal environments of an epeiric sea may have happened (e.g., Tang et al., 2014), but there is no evidence for basin isolation in a broad scale on the North China platform. The temporal changes in Ce/Ce*, $Pr_{(SN)}/Yb_{(SN)}$ and Y/Ho ratios occur in Member-IV of the Gaoyuzhuang Formation (~1.54 Ga, Fig. 6), from which abundant microbialites and stromatolites indicate normal shallow-marine environments. Thus, we believe that the mid-Proterozoic North China platform had open-ocean connections and the observed changes in Ce/Ce*, $Pr_{(SN)}/Yb_{(SN)}$ and Y/Ho ratios record secular changes in seawater chemistry.

5.2. REE + Y signatures of the mid-Proterozoic North China platform

The positive Ce anomalies observed in ironstones of the Chuanlinggou Formation indicate that there were redox cycling of Ce in the water column. There must have existed suboxic–oxic surface water so that Ce(IV) carried by Mn–Fe oxides, organic matter and clay minerals went through reductive dissolution and accumulated as reduced Ce(III) below the chemocline (Byrne and Sholkovitz, 1996). In addition, the highly variable light-to-heavy REE ratios of ironstones suggest deposition around the chemocline (cf. Planavsky et al., 2010; Tang et al., 2015). Sedimentological evidence indicates that the oolitic and stromatolitic ironstones (Fig. 3A and B) of the Chuanlinggou Formation were deposited in shallow subtidal environments above fair-weather wave base (Dai et al., 2004; Tang et al., 2015). Thus, we infer that the Fe–Mn redoxcline must have been very shallow.

However, the absence of negative Ce anomalies in carbonates prior to ~1.54 Ga, independent of sedimentary facies (Fig. 6A and B), implies that Ce redox cycling in shallow-marine environments of the early Mesoproterozoic ocean may have been minimum and shallow waters were largely in reduced state relative to Ce. The negative Ce anomalies in younger carbonates (Fig. 6A and B) indicate increasing oxidizing conditions that allowed for significant

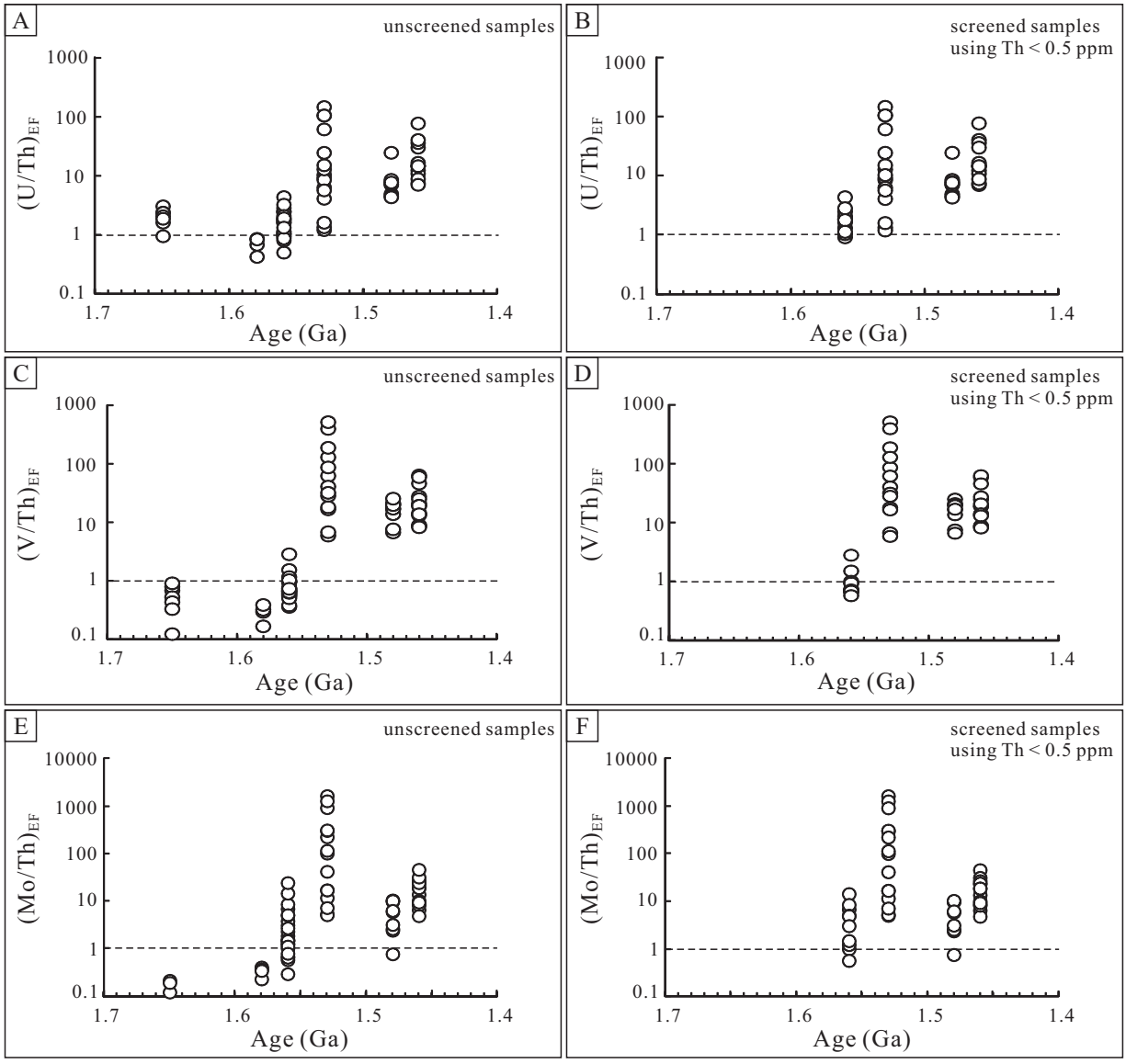

Fig. 7. Temporal trends in U_{EF}, V_{EF}, and Mo_{EF} of ca. 1.65–1.47 Ga ironstones and carbonates showing low values before ~1.54 Ga (close to that of the average upper continental crust) and a simultaneously increase at ~1.54 Ga. Dash line indicates the average upper continental crust value.

Ce redox cycling in shallow waters. The change of Ce anomaly around ~1.54 Ga corresponds well with the secular variation in atmospheric oxygen concentration recorded by Zn/Fe ratios in shallow water carbonates (Liu et al., 2016) and the increase of biotic abundance, diversity and size (Shi et al., 2014).

The minimum oxygen requirement for Ce redox cycling may provide information about the surface ocean dissolved O_2 and atmosphere pO_2 level during the mid-Proterozoic. As Ce(III) has a redox potential close to Mn(II) ($Ce^{3+} - e^- \rightarrow Ce^{4+}$, $E^\circ = +1.61$ V; $Mn^{2+} + 2H_2O \rightarrow MnO_2 + 4H^+ + 2e^-$, $E^\circ = +1.23$ V), this implies that the shallow subtidal environments on the North China platform prior to ~1.54 Ga remained reduced relative to Mn. Based on experiments and numerical modeling, Schippers et al. (2005) concluded that rapid Mn(II) oxidation would happen at an *in situ* O_2 concentration of 0.5 μM and even at the O_2 level of ~0.2 μM, Mn(II) was completely oxidized in their incubations. The general lack of Ce anomalies in the sedimentary rocks prior to ~1.54 Ga probably suggests that free O_2 in shallow subtidal and intertidal waters was below the Mn(II) oxidation minimum (~0.2 μM), given that Ce(III) and Mn(II) oxidation shares a common pathway (Moffett, 1994) and requires similar minimum oxygen level (Planavsky et al., 2010).

Ironstones from the Chuanlinggou Formation were deposited in shallow water environments above fair-weather wave base (Tang et al., 2015), and many carbonate layers in the second and third members of the Gaoyuzhuang Formation are also deposited from shallow subtidal to intertidal environments (Table S1). In depositional environments above fair-weather wave base, wave activities and tides would allow efficient water–atmosphere exchange to have oxygen equilibrium between atmosphere and shallow waters of the ocean. Considering that at normal temperatures, the oxygen content in shallow-marine waters is proportional to atmospheric oxygen level (e.g., Forstner and Gnaiger, 1983), if the oxygen concentration in shallow subtidal and intertidal environments prior to ~1.54 Ga was <0.2 μM (suboxic to anoxic), which is about 0.1% of the modern oxygenated surface ocean (~280 μM; Luther et al., 1991; Sperling et al., 2013), we infer that the atmosphere O_2 level may have also been <0.1% PAL. This is consistent with the estimate of ~0.1% PAL of oxygen for the mid-Proterozoic atmosphere on the basis of chromium isotopes (Planavsky et al., 2014). The low

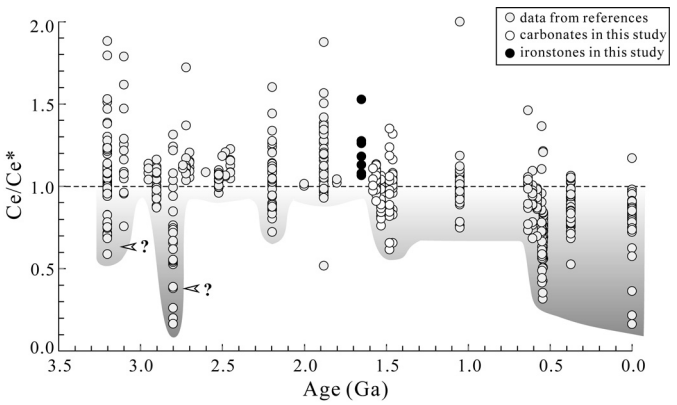

Fig. 8. Temporal trends in Ce anomalies of BIF, ironstones, and carbonates through time, compiled from the data of this study and available data from literature (Table S1; Kato et al., 1996, 1998, 2002; Alibo and Nozaki, 1999; Webb and Kamber, 2000; Nothdurft et al., 2004; Alexander et al., 2008; Azmy et al., 2009; Planavsky et al., 2010; Ling et al., 2013; Tang et al., 2013b). Question marks pointed to negative Ce anomalies from Archean that have been questioned by Planavsky et al. (2010).

(<0.1% PAL) oxygen level is also in agreement with the estimation of low oceanic sulfate level (~1.8 mM) in the mid-Proterozoic ocean (Luo et al., 2015).

The first appearance of negative Ce anomalies in Member-IV of the Gaoyuzhuang Formation indicates that the Mn-redoxcline was deepened toward deep subtidal zone. Considering that there are no significant temporal changes in water depth of the depositional environments, the episodic occurrences of negative Ce anomalies in younger carbonates may suggest that the surface ocean was weakly oxygenated (O_2 >0.2 μM, suboxic) after ~1.54 Ga, with oxygen concentration fluctuated around 0.2 μM.

Similar to the behavior of Ce, in oxic waters light REEs are depleted due to preferential removal of light REEs by Mn–Fe oxides, organic matter and clay particles. The light to heavy REE ratio ($Pr_{(SN)}/Yb_{(SN)}$) increases markedly across Mn–Fe redox boundaries due to reductive dissolution of settling Mn–Fe oxides (Sholkovitz and Elderfield, 1988; German et al., 1991; Sholkovitz et al., 1992; Byrne and Sholkovitz, 1996). Thus, light to heavy REE ratios below the Mn and Fe redox boundaries in many redox-stratified basins are close to or even higher than that of PAAS (de Baar et al., 1988; Schijf et al., 1995; Bau et al., 1997; De Carlo and Green, 2002). In oxic waters, Y/Ho ratios are higher than that of PAAS, due to lower particle-reactivity of Y than its geochemical analog Ho (Bau et al., 1997; Nozaki et al., 1997). In suboxic to anoxic waters, however, Y/Ho ratios would decrease because of more efficient release of Ho relative to Y under reduced conditions (Bau et al., 1997). Therefore, low $Pr_{(SN)}/Yb_{(SN)}$ and high Y/Ho ratios of carbonates indicate more oxic conditions, whereas high $Pr_{(SN)}/Yb_{(SN)}$ and low Y/Ho ratios suggest suboxic to anoxic conditions. The temporal trends in $Pr_{(SN)}/Yb_{(SN)}$ and Y/Ho ratios are very similar to that of the Ce anomaly (Fig. 6C–F). Particularly, the decrease in $Pr_{(SN)}/Yb_{(SN)}$ and increase in Y/Ho ratios at ~1.54 Ga suggest increase in oxygen concentration of the surface water, consistent with the presence of negative Ce anomalies at the same stratigraphic level (Fig. 6C–F).

5.3. RSE signatures of the mid-Proterozoic North China platform

Trace-metal enrichments in marine carbonates may also provide information about the water-column redox state (e.g., Hood and Wallace, 2014, 2015; Sansjofre et al., 2014). Although RSE concentrations can be complicated by diagenetic alterations and we cannot preclude the diagenetic influences on the absolute U_{EF}, V_{EF}, and Mo_{EF} values of our samples, the temporal trends of U_{EF}, V_{EF}, and Mo_{EF} (Fig. 7) may record changes in RSE availability in the depositional water column because our samples were collected from stratigraphically adjacent units that may have experienced similar burial diagenesis.

Numerous studies have shown that seawater RSE concentrations are controlled by the redox landscape of the global ocean, which exerts the first-order control on RSE enrichments in sediments (e.g., Emerson and Huested, 1991; Hastings et al., 1996; Algeo and Lyons, 2006; Scott et al., 2008; Sahoo et al., 2012; Reinhard et al., 2013). Following this reasoning, the increase of U_{EF}, V_{EF}, and Mo_{EF} in Gaoyuzhuang Member IV (Fig. 7) may record expansion of the marine RSE reservoirs in response to more oxic oceans at and after ~1.54 Ga. However, because carbonates are not the efficient RSE carrier during deposition and the lower oxygen level (around 0.2 μM) estimated from Ce/Ce* data do not support a highly oxygenated ocean, we interpret that the increase of U_{EF}, V_{EF}, and Mo_{EF} at ca. 1.54 Ga may record a more vigorous redox-cycling environments for RSEs and/or more active microbial uptake of RSEs during deposition of the Gaoyuzhuang Member-IV. This is consistent with the temporal trend of REE + Y pattern (Fig. 7) and the occurrence of thick, reef-making microbialites in Member-IV of the Gaoyuzhuang Formation.

5.4. Low oxygen concentration as a cause for the evolutionary stasis of eukaryotes

Recent studies indicate that eukaryotes can survive and even thrive under extremely low oxygen levels (e.g., Sperling et al., 2013; Mills et al., 2014). Theoretical estimate of the minimum O_2 requirement for the last common ancestor of bilaterians ranges from 0.14% to 0.36% PAL (ca. 0.37–0.95 μM), depending on the organism's sizes and possession of a vascular system (Sperling et al., 2013). In the modern ocean, bilaterian faunas can exist in the oxygen-minimum zone of Chile (Palma et al., 2005), Peru (Levin et al., 2002) and the Bay of Bengal (Sperling et al., 2013) with O_2 concentrations as low as ~0.88 μM. Previous studies estimated that the atmospheric oxygen concentration might have varied from 1% to 40% PAL after GOE (Rye and Holland, 1998; Canfield, 2005; Holland, 2006; Kump, 2008; Reinhard et al., 2013), which are well above the oxygen demands of the metazoan ancestors before NOE (Mills et al., 2014). For this reason, some researchers argued that the origin of metazoans may not have been directly related to the rise of oxygen in Earth's surface environments (e.g., Mills et al., 2014).

A recent chromium isotope study indicates that atmospheric oxygen levels during the mid-Proterozoic were probably lower than 0.1% PAL (Planavsky et al., 2014), far below the minimum O_2 requirement of most multicellular animals (Sperling et al., 2013; Mills et al., 2014). Our REE + Y data provide additional evidence that supports low oxygen levels in mid-Proterozoic atmosphere and ocean. The dissolved oxygen in shallow-marine environments may have been below 0.2 μM during the latest Paleoproterozoic to early Mesoproterozoic, with a marked increase at ~1.54 Ga and fluctuating levels thereafter. This implies that, when looking into the details, the ocean oxygenation may have been more complicated than an overly simplified two-step oxygenation (Canfield et al., 2013; Asael et al., 2013; Lyons et al., 2014), even in the Mesoproterozoic era when atmospheric oxygen level was very low in general (e.g., Sperling et al., 2013; Reinhard et al., 2013; Planavsky et al., 2014). Low oxygen levels would have limited organisms to small sizes and thin body plans with little metabolic scope (e.g., Payne et al., 2011; Sperling et al., 2013), which would in turn exert impact on the multi-cellularity and diversification of eukaryotes (Schirrmeister et al., 2013). Our results suggest that the low oxygen level in surface oceans could have played a crucial role in the evolution of eukaryotes and help explain the billion-year-long evolutionary stasis during the mid-Proterozoic

and delayed appearance of metazoans until the terminal Proterozoic.

6. Conclusion

Shallow-marine ironstones and carbonates from latest Paleoproterozoic to early Mesoproterozoic strata of the North China platform were investigated for their REE + Y patterns and trace-element concentrations. The lack of negative Ce anomalies in shallow-water carbonates prior to ~1.54 Ga suggests low oxygen concentration (<0.2 μM) in shallow-marine environments that limited Ce (and Mn) redox cycling. The presence of episodic negative Ce anomalies in shallow-water carbonates after ~1.54 Ga suggests increase of surface-water oxygen concentrations, but frequent shifts in Ce/Ce* between carbonates of identical depositional water depth imply that shallow chemocline possibly remained through most of the mid-Proterozoic. The coincident occurrence of negative Ce anomalies, decrease in $Pr_{(SN)}/Yb_{(SN)}$ ratios, increase in Y/Ho ratios, and increase in U_{EF}, V_{EF}, and Mo_{EF} at ~1.54 Ga suggests an Oxygenation Event, although its global significance requires further investigation. The low oxygen level in shallow seawater (~0.2 μM) estimated from the REE data support that low oxygen was the major barrier for eukaryotic diversification during the mid-Proterozoic and helps explain the delayed evolution of metazoans until terminal Proterozoic.

Acknowledgments

The study was supported by the Ministry of Science and Technology (No. 2011CB808806), the National Natural Science Foundation of China (Nos. 41272039 and 41402024), and by China University of Geosciences, Beijing (No. 2652014063). We appreciate Mr. Zhao G. and Li T. for their partly assistance in field work. We are grateful to the very thoughtful comments provided by two anonymous reviewers that helped improve the manuscript.

Appendix A. Supplementary data

Supplementary data associated with this article can be found, in the online version, at http://dx.doi.org/10.1016/j.precamres.2016.02.005.

References

Alexander, B.W., Bau, M., Andersson, P., Dulski, P., 2008. Continentally-derived solutes in shallow Archean seawater: rare earth element and Nd isotope evidence in iron formation from the 2.9 Ga Pongola Supergroup, South Africa. Geochim. Cosmochim. Acta 72, 378–394.

Algeo, T.J., Lyons, T.W., 2006. Mo–total organic carbon covariation in modern anoxic marine environments: implications for analysis of paleoredox and paleohydrographic conditions. Paleoceanography, http://dx.doi.org/10.1029/2004PA001112, 21PA1016.

Alibo, D.S., Nozaki, Y., 1999. Rare earth elements in seawater: particle association, shale-normalization, and Ce oxidation. Geochim. Cosmochim. Acta 63, 363–372.

Anbar, A.D., Knoll, A.H., 2002. Proterozoic ocean chemistry and evolution: a bioinorganic bridge? Science 297, 1137–1143.

Asael, D., Tissot, F.L., Reinhard, C.T., Rouxel, O., Dauphas, N., Lyons, T.W., Ponzevera, E., Liorzou, C., Chéron, S., 2013. Coupled molybdenum, iron and uranium stable isotopes as oceanic paleoredox proxies during the Paleoproterozoic Shunga Event. Chem. Geol. 362, 193–210.

Azmy, K., Sylvester, P., de Oliveira, T.F., 2009. Oceanic redox conditions in the Late Mesoproterozoic recorded in the upper Vazante Group carbonates of São Francisco Basin, Brazil: evidence from stable isotopes and REEs. Precambrian Res. 168, 259–270.

Banner, J.L., Hanson, G.N., Meyers, W.J., 1988. Rare earth element and Nd isotopic variations in regionally extensive dolomites from the Burlington-Keokuk Formation (Mississippian): implications for REE mobility during carbonate diagenesis. J. Sediment. Res. 58, 415–432.

Bartley, J.K., Kah, L.C., Frank, T.D., Lyons, T.W., 2015. Deep-water microbialites of the Mesoproterozoic Dismal Lakes Group: microbial growth, lithification, and implications for coniform stromatolites. Geobiology 13, 15–32.

Bau, M., 1993. Effects of syn-and post-depositional processes on the rare-earth element distribution in Precambrian iron-formations. Eur. J. Mineral. 5, 257–267.

Bau, M., Dulski, P., 1996. Distribution of yttrium and rare-earth elements in the Penge and Kuruman Iron-Formations, Transvaal Supergroup, South Africa. Precambrian Res. 79, 37–55.

Bau, M., Koschinsky, A., Dulski, P., Hein, J.R., 1996. Comparison of the partitioning behaviours of yttrium, rare earth elements, and titanium between hydrogenetic marine ferromanganese crusts and seawater. Geochim. Cosmochim. Acta 60, 1709–1725.

Bau, M., Möller, P., Dulski, P., 1997. Yttrium and lanthanides in eastern Mediterranean seawater and their fractionation during redox-cycling. Mar. Chem. 56, 123–131.

Bau, M., Möller, P., 1993. Rare-earth element systematics of the chemically precipitated component in early Precambrian Fe Formations and the evolution of the terrestrial atmosphere–hydrosphere–lithosphere system. Geochim. Cosmochim. Acta 57, 2239–2249.

Bekker, A., Holland, H.D., 2012. Oxygen overshoot and recovery during the early Paleoproterozoic. Earth Planet. Sci. Lett. 317–318, 295–304.

Bekker, A., Holland, H.D., Wang, P.L., Rumble III, D., Stein, H.J., Hannah, J.L., Coetzee, L.L., Beukes, N.J., 2004. Dating the rise of atmospheric oxygen. Nature 427, 117–120.

Bertram, C.J., Elderfield, H., 1993. The geochemical balance of the rare-earth elements and neodymium isotopes in the oceans. Geochim. Cosmochim. Acta 57, 1957–1986.

Blumenberg, M., Thiel, V., Riegel, W., Kah, L.C., Reitner, J., 2012. Black shale formation by microbial mats lacking sterane-producing eukaryotes, late Mesoproterozoic (1.1 Ga) Taoudeni Basin, Mauritania. Precambrian Res. 196–197, 113–127.

Brocks, J.J., Love, G.D., Summons, R.E., Knoll, A.H., Logan, G.A., Bowden, S.A., 2005. Biomarker evidence for green and purple sulphur bacteria in a stratified Palaeoproterozoic sea. Nature 437, 866–870.

Butterfield, N.J., 2000. *Bangiomorpha pubescens* n. gen., n. sp.: implications for the evolution of sex, multicellularity, and the Mesoproterozoic/Neoproterozoic radiation of eukaryotes. Paleobiology 26, 386–404.

Butterfield, N.J., 2001. Paleobiology of the late Mesoproterozoic (ca. 1200 Ma) hunting formation, Somerset Island, Arctic Canada. Precambrian Res. 111, 235–256.

Butterfield, N.J., 2009. Oxygen, animals and oceanic ventilation: an alternative view. Geobiology 7, 1–7.

Byrne, R.H., Sholkovitz, E.R., 1996. Marine chemistry and geochemistry of the lanthanides. In: Gschneidner, K.A., Eyring, L. (Eds.), Handbook on the Physics and Chemistry of Rare Earths. Elsevier, Amsterdam, pp. 497–593.

Canfield, D.E., 1998. A new model for Proterozoic ocean chemistry. Nature 396, 450–453.

Canfield, D.E., 2005. The early history of atmospheric oxygen: homage to Robert M. Garrels. Annu. Rev. Earth Planet. Sci. 33, 1–36.

Canfield, D.E., Ngombi-Pemba, L., Hammarlund, E.U., Bengtson, S., Chaussidon, M., Gauthier-Lafaye, F., Meunier, A., Riboulleau, A., Rollion-Bard, C., Rouxel, O., Asael, D., Pierson-Wickmann, A., El Albani, A., 2013. Oxygen dynamics in the aftermath of the Great Oxidation of Earth's atmosphere. Proc. Natl. Acad. Sci. U. S. A. 110, 16736–16741.

Canfield, D.E., Poulton, S.W., Knoll, A.H., Narbonne, G.M., Ross, G., Goldberg, T., Strauss, H., 2008. Ferruginous conditions dominated later Neoproterozoic deep-water chemistry. Science 321, 949–952.

Canfield, D.E., Poulton, S.W., Narbonne, G.M., 2007. Late-Neoproterozoic deep-ocean oxygenation and the rise of animal life. Science 315, 92–95.

Canfield, D.E., Teske, A., 1996. Late Proterozoic rise in atmospheric oxygen concentration inferred from phylogenetic and sulphur-isotope studies. Nature 382, 127–132.

Chu, X.L., Zhang, T.G., Zhang, Q.R., Lyons, T.W., 2007. Sulfur and carbon isotope records from 1700 to 800 Ma carbonates of the Jixian section, northern China: implications for secular isotope variations in Proterozoic seawater and relationships to global supercontinental events. Geochim. Cosmochim. Acta 71, 4668–4692.

Dai, Y.D., Song, H.M., Shen, J.Y., 2004. Fossil bacteria in Xuanlong iron ore deposits of Hebei Province. Sci. China (Earth Sci.) 47, 347–356.

de Baar, H.J.W., German, C.R., Elderfield, H., Vangaans, P., 1988. Rare-earth element distributions in anoxic waters of the Cariaco Trench. Geochim. Cosmochim. Acta 52, 1203–1219.

De Carlo, E.H., Green, W.J., 2002. Rare earth elements in the water column of Lake Vanda, McMurdo Dry Valleys, Antarctica. Geochim. Cosmochim. Acta 66, 1323–1333.

Duan, C., Li, Y.H., Wei, M.H., Yang, Y., Hou, K.J., Chen, X.D., Zhou, B., 2014. U–Pb dating study of detrital zircons from the Chuanlinggou Formation in Jiangjiazhai iron deposit, North China Craton and its geological significances. Acta Petrol. Sin. 30, 35–48 (in Chinese with English abstract).

Elderfield, H., Hawkesworth, C.J., Greaves, M.J., Calvert, S.E., 1981. Rare earth element zonation in Pacific ferromanganese nodules. Geochim. Cosmochim. Acta 45, 1231–1234.

Emerson, S.R., Huested, S.S., 1991. Ocean anoxia and the concentrations of molybdenum and vanadium in seawater. Mar. Chem. 34, 177–196.

Erwin, D.H., Laflamme, M., Tweedt, S.M., Sperling, E.A., Pisani, D., Peterson, K.J., 2011. The Cambrian conundrum: early divergence and later ecological success in the early history of animals. Science 334, 1091–1097.

Farquhar, J., Bao, H.M., Thiemens, M., 2000. Atmospheric influence of Earth's earliest sulfur cycle. Science 289, 756–758.

Fike, D.A., Grotzinger, J.P., Pratt, L.M., Summons, R.E., 2006. Oxidation of the Ediacaran Ocean. Nature 444, 744–747.

Forstner, H., Gnaiger, E., 1983. Calculation of equilibrium oxygen concentration. In: Gnaiger, E., Forstner, H. (Eds.), Polarographic Oxygen Sensors. Springer, Berlin, pp. 321–333.
Gao, L.Z., Ding, X.Z., Gao, Q., Zhang, C.H., 2010. New geological time scale of Late Precambrian in China and geochronology. Geol. China 37, 1014–1020 (in Chinese with English abstract).
Gao, L.Z., Zhang, C.H., Liu, P.J., Ding, X.Z., Wang, Z.Q., Zhang, Y.J., 2009. Recognition of Meso- and Neoproterozoic stratigraphic framework in North and South China. Acta Geosci. Sin. 30, 433–446 (in Chinese with English abstract).
Gao, L.Z., Zhang, C.H., Shi, X.Y., Song, B., Wang, Z.Q., Liu, Y.M., 2008a. Mesoproterozoic age for Xiamaling Formation in North China plate indicated by zircon SHRIMP dating. Chin. Sci. Bull. 53, 2665–2671.
Gao, L.Z., Zhang, C.H., Shi, X.Y., Zhou, H.R., Wang, Z.Q., 2007. Zircon SHRIMP U–Pb dating of the tuff bed in the Xiamaling Formation of the Qingbaikouan System in North China. Geol. Bull. China 26, 249–255 (in Chinese with English abstract).
Gao, L.Z., Zhang, C.H., Yin, C.Y., Shi, X.Y., Wang, Z.Q., Liu, Y.M., Liu, P.J., Tang, F., Song, B., 2008b. SHRIMP zircon ages: basis for refining the chronostratigraphic classification of the Meso- and Neoproterozoic strata in North China old land. Acta Geosci. Sin. 29, 366–376 (in Chinese with English abstract).
German, C.R., Elderfield, H., 1989. Rare earth elements in Saanich Inlet, British Columbia, a seasonally anoxic basin. Geochim. Cosmochim. Acta 53, 2561–2571.
German, C.R., Holliday, B.P., Elderfield, H., 1991. Redox cycling of rare earth elements in the suboxic zone of the Black Sea. Geochim. Cosmochim. Acta 55, 3553–3558.
German, C.R., Masuzawa, T., Greaves, M.J., Elderfield, H., Edmond, J.M., 1995. Dissolved rare-earth elements in the Southern Ocean: cerium oxidation and the influence of hydrography. Geochim. Cosmochim. Acta 59, 1551–1558.
Gilleaudeau, G.J., Kah, L.C., 2015. Heterogeneous redox conditions and a shallow chemocline in the Mesoproterozoic ocean: evidence from carbon–sulfur–iron relationships. Precambrian Res. 257, 94–108.
Guo, H., Du, Y.S., Huang, J.H., Yang, J.H., Huang, H., Chen, Y., Zhou, Y., 2010. Habitat types and palaeoenvironments of the Mesoproterozoic Gaoyuzhuang Formation in Pingquan, Hebei Province. J. Palaeogeogr. 12, 269–280 (in Chinese with English abstract).
Guo, H., Du, Y.S., Kah, L.C., Huang, J.H., Hu, C.Y., Huang, H., Yu, W.C., 2013a. Isotopic composition of organic and inorganic carbon from the Mesoproterozoic Jixian Group, North China: implications for biological and oceanic evolution. Precambrian Res. 224, 169–183.
Guo, H., Du, Y.S., Lian, Z., Yang, J.H., Huang, H., 2013b. Trace and rare earth elemental geochemistry of carbonate succession in the Middle Gaoyuzhuang Formation, Pingquan Section: implications for Early Mesoproterozoic ocean redox conditions. J. Palaeogeogr. 2, 209–221, http://dx.doi.org/10.3724/SP.J.1261.2013.00027.
Han, T.M., Runnegar, B., 1992. Megascopic eukaryotic algae from the 2.1-billion-year-old Negaunee Iron-Formation, Michigan. Science 257, 232–235.
Hardisty, D.S., Lu, Z., Planavsky, N.J., Bekker, A., Philippot, P., Zhou, X., Lyons, T.W., 2014. An iodine record of Paleoproterozoic surface ocean oxygenation. Geology 42, 619–622.
Hastings, D.W., Emerson, S.R., Mix, A.C., 1996. Vanadium in foraminiferal calcite as a tracer for changes in the areal extent of reducing sediments. Paleoceanography 11, 665–678.
Holland, H.D., 2002. Volcanic gases, black smokers, and the great oxidation event. Geochim. Cosmochim. Acta 66, 3811–3826.
Holland, H.D., 2006. The oxygenation of the atmosphere and oceans. Philos. Trans. R. Soc. B: Biol. Sci. 361, 903–915.
Hood, A.V.S, Wallace, M.W., 2014. Marine cements reveal the structure of an anoxic, ferruginous Neoproterozoic ocean. J. Geol. Soc. 171, 741–744.
Hood, A.V.S., Wallace, M.W., 2015. Extreme ocean anoxia during the Late Cryogenian recorded in reefal carbonates of Southern Australia. Precambrian Res. 261, 96–111.
Javaux, E.J., Knoll, A.H., Walter, M.R., 2001. Morphological and ecological complexity in early eukaryotic ecosystems. Nature 412, 66–69.
Johnston, D.T., Poulton, S.W., Tosca, N.J., O'Brien, T., Halverson, G.P., Schrag, D.P., Macdonald, F.A., 2013. Searching for an oxygenation event in the fossiliferous Ediacaran of northwestern Canada. Chem. Geol. 362, 273–286.
Kamber, B.S., Webb, G.E., 2001. The geochemistry of late Archaean microbial carbonate: implications for ocean chemistry and continental erosion history. Geochim. Cosmochim. Acta 65, 2509–2525.
Kato, Y., Kano, T., Kunugiza, K., 2002. Negative Ce anomaly in the Indian banded iron formations: evidence for the emergence of oxygenated deep-sea at 2.9–2.7 Ga. Resour. Geol. 52, 101–110.
Kato, Y., Kawakami, T., Kano, T., Kunugiza, K., Swamy, N.S., 1996. Rare-earth element geochemistry of banded iron formations and associated amphibolite from the Sargur belts, south India. J. Southeast Asian Earth Sci. 14, 161–164.
Kato, Y., Ohta, I., Tsunematsu, T., Watanabe, Y., Isozaki, Y., Maruyama, S., Imai, N., 1998. Rare earth element variations in mid-Archean banded iron formations: implications for the chemistry of ocean and continent and plate tectonics. Geochim. Cosmochim. Acta 62, 3475–3497.
Kendall, B., Komiya, T., Lyons, T.W., Bates, S.M., Gordon, G.W., Romaniello, S.J., Jiang, G.Q., Creaser, R.A., Xiao, S.H., McFadden, K., Sawaki, Y., Tahata, M., Shu, D.G., Han, J., Li, Y., Chu, X.L., Anbar, A.D., 2015. Uranium and molybdenum isotope evidence for an episode of widespread ocean oxygenation during the late Ediacaran Period. Geochim. Cosmochim. Acta 156, 173–193.
Knoll, A.H., Javaux, E.J., Hewitt, D., Cohen, P., 2006. Eukaryotic organisms in Proterozoic oceans. Philos. Trans. R. Soc. B: Biol. Sci. 361, 1023–1038.
Knoll, A.H., Kaufman, A.J., Semikhatov, M.A., 1995. The carbon-isotopic composition of Proterozoic carbonates: Riphean successions from north-western Siberia (Anabar Massif, Turukhansk Uplift). Am. J. Sci. 295, 823–850.
Kump, L.R., 2008. The rise of atmospheric oxygen. Nature 451, 277–278.
Kurzweil, F., Drost, K., Pašava, J., Wille, M., Taubald, H., Schoeckle, D., Schoenberg, R., 2015. Coupled sulfur iron and molybdenum isotope data from black shales of the Teplá-Barrandian unit argue against deep ocean oxygenation during the Ediacaran. Geochim. Cosmochim. Acta 171, 121–142.
Lamb, D.M., Awramik, S.M., Chapman, D.J., Zhu, S.X., 2009. Evidence for eukaryotic diversification in the ca. 1800 million-year-old Changzhougou Formation, North China. Precambrian Res. 173, 93–104.
Lawrence, M.G., Greig, A., Collerson, K.D., Kamber, B.S., 2006. Rare earth element and yttrium variability in South East Queensland waterways. Aquat. Geochem. 12, 39–72.
Levin, L., Gutiérrez, D., Rathburn, A., Neira, C., Sellanes, J., Munoz, P., Gallardob, V., Salamanca, M., 2002. Benthic processes on the Peru margin: a transect across the oxygen minimum zone during the 1997–98 El Niño. Prog. Oceanogr. 53, 1–27.
Li, C., Peng, P.A., Sheng, G.Y., Fu, J.M., Yan, Y.Z., 2003. A molecular and isotopic geochemical study of Meso-to Neoproterozoic (1. 73–0.85 Ga) sediments from the Jixian section, Yanshan Basin North China. Precambrian Res. 125, 337–356.
Li, H.K., Su, W.B., Zhou, H.Y., Xiang, Z.Q., Tian, H., Yang, L.G., Huff, W.D., Ettensohn, F.R., 2014. The first precise age constraints on the Jixian System of the Meso- to Neoproterozoic Standard Section of China: SHRIMP zircon U–Pb dating of bentonites from the Wumishan and Tieling formations in the Jixian Section, North China Craton. Acta Petrol. Sin. 30, 2999–3012.
Li, C., Planavsky, N.J., Love, G.D., Reinhard, C.T., Hardisty, D., Feng, L., Bates, S.M., Huang, J., Zhang, Q.R., Chu, X.L., Lyons, T.W., 2015. Marine redox conditions in the middle Proterozoic ocean and isotopic constraints on authigenic carbonate formation: insights from the Chuanlinggou Formation, Yanshan Basin, North China. Geochim. Cosmochim. Acta 150, 90–105.
Li, H.K., Lu, S.N., Su, W.B., Xiang, Z.Q., Zhou, H.Y., Zhang, Y.Q., 2013. Recent advances in the study of the Mesoproterozoic geochronology in the North China Craton. J. Asian Earth Sci. 72, 216–227.
Li, H.K., Zhu, S.X., Xiang, Z.Q., Su, W.B., Lu, S.N., Zhou, H.Y., Geng, J.Z., Li, S., Yang, F.J., 2010. Zircon U–Pb dating on tuff bed from Gaoyuzhuang formation in Yanqing, Beijing: further constraints on the new subdivision of the Mesoproterozoic stratigraphy in the northern North China Craton. Acta Petrol. Sin. 2, 2131–2140 (in Chinese with English abstract).
Li, X.H., Li, W.X., Li, Z.X., Liu, Y., 2008. 850–790 Ma bimodal volcanic and intrusive rocks in northern Zhejiang, South China: a major episode of continental rift magmatism during the breakup of Rodinia. Lithos 102, 341–357.
Ling, H.F., Chen, X., Li, D., Wang, D., Shields-Zhou, G.A., Zhu, M.Y., 2013. Cerium anomaly variations in Ediacaran–earliest Cambrian carbonates from the Yangtze Gorges area, South China: implications for oxygenation of coeval shallow seawater. Precambrian Res. 225, 110–127.
Liu, X.M., Kah, L.C., Knoll, A.H., Cui, H., Kaufman, A.J., Shahar, A., Hazen, R.M., 2016. Tracing Earth's O_2 evolution using Zn/Fe ratios in marine carbonates. Geochem. Perspect. Lett. 2, 24–34.
Lu, S.N., Li, H.M., 1991. A precise U–Pb single zircon age determination for the volcanics of Dahongyu Formation, Changcheng system in Jixian. Acta Geosci. Sin. 22, 137–145 (in Chinese with English abstract).
Lu, S.N., Yang, C.L., Li, H.K., Li, H.M., 2002. A group of rifting events in the terminal Paleoproterozoic in the North China Craton. Gondwana Res. 5, 123–131.
Lu, S.N., Zhao, G.C., Wang, H.C., Hao, G.J., 2008. Precambrian metamorphic basement and sedimentary cover of the North China Craton: a review. Precambrian Res. 160, 77–93.
Luo, G.M., Junium, C.K., Kump, L.R., Huang, J.H., Li, C., Feng, Q.L., Shi, X.Y., Bai, X., Xie, S.C., 2014. Shallow stratification prevailed for ~1700 to ~1300 Ma ocean: evidence from organic carbon isotopes in the North China Craton. Earth Planet. Sci. Lett. 400, 219–232.
Luo, G.M., Ono, S., Huang, J.H., Algeo, T.J., Li, C., Zhou, L., Robinson, A., Lyons, T.W., Xie, S.C., 2015. Decline in oceanic sulfate levels during the early Mesoproterozoic. Precambrian Res. 258, 36–47.
Luther III, G.W., Church, T.M., Powell, D., 1991. Sulfur speciation and sulfide oxidation in the water column of the Black-Sea. Deep-Sea Res. 38, S1121–S1137.
Lyons, T.W., Reinhard, C.T., Planavsky, N.J., 2014. The rise of oxygen in Earth's early ocean and atmosphere. Nature 506, 307–315.
Mei, M.X., 2007. Implications of the Precambrian non-stromatolitic carbonate succession making up the third member of Mesoproterozoic Gaoyuzhuang Formation in Yanshan Area of North China. J. China Univ. Geosci. 18, 191–209.
Mei, M.X., 2008. Sedimentary features and implications for the Precambrian non-stromatolitic carbonate succession: a case study of the Mesoproterozoic Gaoyuzhuang Formation at the Qiangou Section in Yanqing County of Beijing. Acta Geol. Sin. 82, 295–309 (English edition).
Mills, D.B., Ward, L.M., Jones, C., Sweeten, B., Forth, M., Treusch, A.H., Canfield, D.E., 2014. Oxygen requirements of the earliest animals. Proc. Natl. Acad. Sci. U. S. A. 111, 4168–4172.
Moffett, J.W., 1994. The relationship between cerium and manganese oxidation in the marine-environment. Limnol. Oceanogr. 39, 1309–1318.
Nesbitt, H.W., 1979. Mobility and fractionation of rare earth elements during weathering of a granodiorite. Nature 279, 206–210.
Nothdurft, L.D., Webb, G.E., Kamber, B.S., 2004. Rare earth element geochemistry of Late Devonian reefal carbonates, Canning basin, Western Australia: confirmation of a seawater REE proxy in ancient limestones. Geochim. Cosmochim. Acta 68, 263–283.

Nozaki, Y., Alibo, D.S., Amakawa, H., Gamo, T., Hasumoto, H., 1999. Dissolved rare earth elements and hydrography in the Sulu Sea. Geochim. Cosmochim. Acta 63, 2171–2181.
Nozaki, Y., Zhang, J., Amakawa, H., 1997. The fractionation between Y and Ho in the marine environment. Earth Planet. Sci. Lett. 148, 329–340.
Och, L.M., Shields-Zhou, G.A., 2012. The Neoproterozoic oxygenation event: environmental perturbations and biogeochemical cycling. Earth Sci. Rev. 110, 26–57.
Olivier, N., Boyet, M., 2006. Rare earth and trace elements of microbialites in Upper Jurassic coral- and sponge-microbialite reefs. Chem. Geol. 230, 105–123.
Palma, M., Quiroga, E., Gallardo, V.A., Arntz, W., Gerdes, D., Schneider, W., Hebbeln, D., 2005. Macrobenthic animal assemblages of the continental margin off Chile (22° to 42°S). J. Mar. Biol. Assoc. U. K. 85, 233–245.
Pavlov, A.A., Kasting, J.F., 2002. Mass-independent fractionation of sulfur isotopes in Archean sediments: strong evidence for an anoxic Archean atmosphere. Astrobiology 2, 27–42.
Payne, J.L., McClain, C.R., Boyer, A.G., Brown, J.H., Finnegan, S., Kowalewski, M., Krause, J.R.A., Lyons, S.K., McShea, D.W., Novack-Gottshall, P.M., Smith, F.A., Spaeth, P., Stempien, J.A., Wang, S.C., 2011. The evolutionary consequences of oxygenic photosynthesis: a body size perspective. Photosynth. Res. 107, 37–57.
Planavsky, N., Bekker, A., Rouxel, O.J., Kamber, B., Hofmann, A., Knudsen, A., Lyons, T.W., 2010. Rare earth element and yttrium compositions of Archean and Paleoproterozoic Fe formations revisited: new perspectives on the significance and mechanisms of deposition. Geochim. Cosmochim. Acta 74, 6387–6405.
Planavsky, N.J., Peter, M.G., Scott, C.T., Chao, L., Reinhard, C.T., Kelly, A.E., Chu, X.L., Bekker, A., Love, G.D., Lyons, T.W., 2011. Widespread iron-rich conditions in the mid-proterozoic ocean. Nature 477, 448–451.
Planavsky, N.J., Reinhard, C.T., Wang, X.L., Thomson, D., McGoldrick, P., Rainbird, R.H., Johnson, T., Fischer, W.W., Lyons, T.W., 2014. Low Mid-Proterozoic atmospheric oxygen levels and the delayed rise of animals. Science 346, 635–638.
Qiao, X.F., Gao, L.Z., 2007. Mesoproterozoic palaeoearthquake and palaeogeography in Yan-Liao Aulacogen. J. Palaeogeogr. 9, 337–352 (in Chinese with English abstract).
Qiao, X.F., Gao, L.Z., Zhang, C.H., 2007. New idea of the Meso- and Neoproterozoic chronostratigraphic chart and tectonic environment in Sino-Korean Plate. Geol. Bull. China 26, 503–509 (in Chinese with English abstract).
Rasmussen, B., Fletcher, I.R., Brocks, J.J., Kilburn, M.R., 2008. Reassessing the first appearance of eukaryotes and cyanobacteria. Nature 455, 1101–1104.
Reinhard, C.T., Planavsky, N.J., Robbins, L.J., Partin, C.A., Gill, B.C., Lalonde, S.V., Bekker, A., Konhauser, K.O., Lyons, T.W., 2013. Proterozoic ocean redox and biogeochemical stasis. Proc. Natl. Acad. Sci. U. S. A. 110, 5357–5362.
Rye, R., Holland, H.D., 1998. Paleosols and the evolution of atmospheric oxygen: a critical review. Am. J. Sci. 298, 621–672.
Sahoo, S.K., Planavsky, N.J., Kendall, B., Wang, X., Shi, X., Scott, C., Anbar, A.D., Lyons, T.W., Jiang, G., 2012. Ocean oxygenation in the wake of the Marinoan glaciation. Nature 489, 546–549.
Sansjofre, P., Trindade, R.I., Ader, M., Soares, J.L., Nogueira, A.C., Tribovillard, N., 2014. Paleoenvironmental reconstruction of the Ediacaran Araras platform (Western Brazil) from the sedimentary and trace metals record. Precambrian Res. 241, 185–202.
Schijf, J., de Baar, H.J.W., Millero, F.J., 1995. Vertical distributions and speciation of dissolved rare earth elements in the anoxic brines of Bannock Basin, eastern Mediterranean. Geochim. Cosmochim. Acta 57, 1419–1432.
Schippers, A., Neretin, L.N., Lavik, G., Leipe, T., Pollehne, F., 2005. Manganese(II) oxidation driven by lateral oxygen intrusions in the western Black Sea. Geochim. Cosmochim. Acta 69, 2241–2252.
Schirrmeister, B.E., de Vos, J.M., Antonelli, A., Bagheri, H.C., 2013. Evolution of multicellularity coincided with increased diversification of cyanobacteria and the Great Oxidation Event. Proc. Natl. Acad. Sci. U. S. A. 110, 1791–1796.
Schröder, S., Grotzinger, J.P., 2007. Evidence for anoxia at the Ediacaran–Cambrian boundary: the record of redox-sensitive trace elements and rare earth elements in Oman. J. Geol. Soc. 164, 175–187.
Scott, C., Lyons, T.W., Bekker, A., Shen, Y., Poulton, S.W., Chu, X., Anbar, A.D., 2008. Tracing the stepwise oxygenation of the Proterozoic ocean. Nature 452, 456–459.
Shi, M., Feng, Q.L., Zhu, S.X., 2014. Biotic evolution and its relation with geological events in the Proterozoic Yanshan Basin, North China. Science China: Earth Sci. 57, 903–918, http://dx.doi.org/10.1007/s11430-014-4830-7.
Shi, X.Y., Zhang, C.H., Jiang, G.Q., Liu, J., Wang, Y., Liu, D.B., 2008. Microbial mats in the Mesoproterozoic carbonates of the north China Platform and their potential for hydrocarbon generation. J. China Univ. Geosci. 19, 549–566.
Shimizu, H., Tachikawa, K., Masuda, A., Nozaki, Y., 1994. Cerium and neodymium isotope ratios and REE patterns in seawater from the North Pacific-Ocean. Geochim. Cosmochim. Acta 58, 323–333.
Sholkovitz, E.R., Elderfield, H., 1988. Cycling of dissolved rare earth elements in Chesapeake Bay. Glob. Biogeochem. Cycl. 2, 157–176.
Sholkovitz, E.R., Schneider, D.L., 1991. Cerium redox cycles and rare earth elements in the Sargasso Sea. Geochim. Cosmochim. Acta 55, 2737–2743.
Sholkovitz, E.R., Shaw, T., Schneider, D.L., 1992. The geochemistry of rare earth elements in the seasonally anoxic water column and porewaters of Chesapeake Bay. Geochim. Cosmochim. Acta 56, 3389–3402.
Slack, J.F., Grenne, T., Bekker, A., Rouxel, O.J., Lindberg, P.A., 2007. Suboxic deep seawater in the late Paleoproterozoic: evidence from hematitic chert and Fe formation related to seafloor-hydrothermal sulfide deposits, central Arizona, USA. Earth Planet. Sci. Lett. 255, 243–256.
Smith, M.P., Harper, D.A., 2013. Causes of the Cambrian explosion. Science 341, 1355–1356.
Sperling, E.A., Wolock, C.J., Morgan, A.S., Gill, B.C., Kunzmann, M., Halverson, G.P., Macdonald, F.A., Knoll, A.H., Johnston, D.T., 2015. Statistical analysis of iron geochemical data suggests limited late Proterozoic oxygenation. Nature 523, 451–454.
Sperling, E.A., Halverson, G.P., Knoll, A.H., Macdonald, F.A., Johnston, D.T., 2013. A basin redox transect at the dawn of animal life. Earth Planet. Sci. Lett. 371, 143–155.
Su, W.B., 2014. A review of the revised Precambrian time scale (GTS2012) and the research of the Mesoproterozoic chronostratigraphy of China. Earth Sci. Front. 21, 119–138.
Su, W.B., Li, H.K., Huff, W.D., Ettensohn, F.R., Zhang, S.H., Zhou, H.Y., Wan, Y.S., 2010. SHRIMP U–Pb dating for a K-bentonite bed in the Tieling Formation, North China. Chin. Sci. Bull. 55, 3312–3323.
Su, W.B., Zhang, S.H., Huff, W.D., Li, H.K., Ettensohn, F.R., Chen, X.Y., Yang, H.M., Han, Y.G., Song, B., Santosh, M., 2008. SHRIMP U–Pb ages of K-bentonite beds in the Xiamaling Formation: implications for revised subdivision of the Meso-to Neoproterozoic history of the North China Craton. Gondwana Res. 14, 543–553.
Tachikawa, K., Jeandel, C., Vangriesheim, A., Dupré, B., 1999. Distribution of rare earth elements and neodymium isotopes in suspended particles of the tropical Atlantic Ocean (EUMELI site). Deep Sea Res. Part I: Oceanogr. Res. Pap. 46, 733–755.
Tanaka, K., Tani, Y., Takahashi, Y., Tanimizu, M., Suzuki, Y., Kozai, N., Ohnuki, T., 2010. A specific Ce oxidation process during sorption of rare earth elements on biogenic Mn oxide produced by *Acremonium* sp. strain KR21-2. Geochim. Cosmochim. Acta 74, 5463–5477.
Tang, D.J., Shi, X.Y., Jiang, G.Q., 2013a. Mesoproterozoic biogenic thrombolites from the North China platform. Int. J. Earth Sci. 102, 401–413.
Tang, D.J., Shi, X.Y., Jiang, G.Q., 2014. Sunspot cycles recorded in Mesoproterozoic carbonate biolaminites. Precambrian Res. 248, 1–16.
Tang, D.J., Shi, X.Y., Liu, D.B., Lin, Y.T., Zhang, C.H., Song, G.Y., Wu, J.J., 2015. Terminal Paleoproterozoic ooidal ironstone from North China: a sedimentary response to the initial breakup of Columbia supercontinent. Earth Sci. J. China Univ. Geosci. 40, 290–304.
Tang, D.J., Shi, X.Y., Pei, Y.P., Jiang, G.Q., Zhao, G.S., 2011. Redox status of the Mesoproterozoic epeiric sea in North China. J. Palaeogeogr. 13, 563–580 (in Chinese with English abstract).
Tang, H.S., Chen, Y.J., Santosh, M., Zhong, H., Yang, T., 2013b. REE geochemistry of carbonates from the Guanmenshan Formation, Liaohe Group, NE Sino-Korean Craton: implications for seawater compositional change during the Great Oxidation Event. Precambrian Res. 227, 316–336.
Tessier, A., Campbell, P.G.C., Bisson, M., 1979. Sequential extraction procedure for the speciation of particulate trace metals. Anal. Chem. 51 (7), 844–851.
Tian, H., Zhang, J., Li, H.K., Su, W.B., Zhou, H.Y., Yang, L.G., Xiang, Z.Q., Geng, J.Z., Liu, H., Zhu, S.X., Xu, Z.Q., 2015. Zircon LA-MC-ICPMS U–Pb dating of tuff from mesoproterozoic Gaoyuzhuang Formation in Jixian County of North China and its geological significance. Acta Geosci. Sin. 36, 647–658.
Van Kranendonk, M.J., Webb, G.E., Kamber, B.S., 2003. Geological and trace element evidence for a marine sedimentary environment of deposition and biogenicity of 3.45 Ga stromatolitic carbonates in the Pilbara Craton, and support for a reducing Archaean ocean. Geobiology 1, 91–108.
Wang, H.Z., Shi, X.Y., Wang, X.L., Yin, H.F., Qiao, X.F., Liu, B.P., Li, S.T., Chen, J.Q., 2000. Research on the Sequence Stratigraphy of China. Guangdong Science and Technology Press, Guangzhou (in Chinese).
Webb, G.E., Kamber, B.S., 2000. Rare earth elements in Holocene reefal microbialites: a new shallow seawater proxy. Geochim. Cosmochim. Acta 64, 1557–1565.
Woods, K., Knoll, A.H., German, T., 1998. Xanthophyte algae from the Mesoproterozoic/Neoproterozoic transition: confirmation of evolutionary implications. Geol. Soc. Am. Abstr. Programs 30, A-232.
Zhang, S.H., Li, Z.X., Evans, D.A.D., Wu, H.C., Li, H.Y., Dong, J., 2012. Pre-Rodinia supercontinent Nuna shaping up: a global synthesis with new paleomagnetic results from North China. Earth Planet. Sci. Lett. 353–354, 145–155.
Zhang, S.H., Zhao, Y., Ye, H., Hu, J.M., Wu, F., 2013. New constraints on ages of the Chuanlinggou and Tuanshanzi formations of the Changcheng System in the Yan-Liao area in the northern North China Craton. Acta Petrol. Sin. 29, 2481–2490.
Zhang, S.C., Wang, X.M., Hammarlund, E.U., Wang, H.J., Costa, M.M., Bjerrum, C.J., Connelly, J.N., Zhang, B.M., Bian, L.Z., Canfield, D.E., 2015. Orbital forcing of climate 1.4 billion years ago. Proc. Natl. Acad. Sci. U. S. A. 112, E1406–E1413.
Zhao, G.C., Li, S.Z., Sun, M., Wilde, S.A., 2011. Assembly, accretion, and break-up of the Palaeo-Mesoproterozoic Columbia supercontinent: records in the North China Craton revisited. Int. Geol. Rev. 53, 1331–1356.
Zhao, G.C., Sun, M., Wilde, S.A., Li, S.Z., 2003. Assembly, accretion and breakup of the Paleo-Mesoproterozoic Columbia supercontinent: records in the North China Craton. Gondwana Res. 6, 417–434.
Zhao, G.C., Sun, M., Wilde, S.A., Li, S.Z., 2004. A Paleo-Mesoproterozoic supercontinent: assembly, growth and breakup. Earth Sci. Rev. 67, 91–123.
Zhou, H.R., Mei, M.X., Luo, Z.Q., Xing, K., 2006. Sedimentary sequence and stratigraphic framework of the Neoproterozoic Qingbaikou system in the Yanshan region, North China. Earth Sci. Front. 13, 280–290 (in Chinese with English abstract).